INTERNATIONAL ATOMIC ENERGY AGENCY
UNITED NATIONS EDUCATIONAL, SCIENTIFIC AND CULTURAL ORGANIZATION
INTERNATIONAL CENTRE FOR THEORETICAL PHYSICS
I.C.T.P., P.O. BOX 586, 34100 TRIESTE, ITALY, CABLE: CENTRATOM TRIESTE

UNITED NATIONS INDUSTRIAL DEVELOPMENT ORGANIZATION

INTERNATIONAL CENTRE FOR SCIENCE AND HIGH TECHNOLOGY
c/o INTERNATIONAL CENTRE FOR THEORETICAL PHYSICS 34100 TRIESTE (ITALY) VIA GRIGNANO, 9 (ADRIATICO PALACE) P.O. BOX 586 TELEPHONE 040-224572 TELEFAX 040-224575 TELEX 460449 APH I

H4.SMR/540-10

Second Training College on Physics and Technology of Lasers and Optical Fibres

21 January - 15 February 1991

OPTOGALVANIC SPECTROSCOPY I

E. Arimondo
Università di Pisa
Dipartimento di Fisica
Pisa, Italy

OPTOGALVANIC AND OPTOACOUSTIC DETECTIONS IN A NEON POSITIVE COLUMN

A. SASSO and M.G. Di VITO
Dipartimento di Fisica Nucleare, Struttura della Materia e Fisica Applicata, Universitá di Napoli, Napoli, Italy

and

E. ARIMONDO
Dipartimento di Fisica, Universitá di Pisa, Pisa, Italy

Received 26 October 1987

The optogalvanic effect in the positive column of a neon discharge is investigated in combination with the simultaneous observations of the optoacoustic effect and the electroacoustic effect, a modification in the discharge temperature produced by an external electrical modulation of the current. The observations of current and power dissipated in the discharge are analyzed through a discharge model for the ionization of neon metastable by electron collisions.

In the optogalvanic (OG) effect in ionized atomic and molecular gases the electrical impedance of an irradiated gas discharge is modified under the irradiation by light in resonance with atomic or molecular transitions of the species present in the discharge. This phenomenon has given new possibilities in high-resolution atomic and molecular spectroscopy, analytical chemistry, plasma diagnostic, laser calibration and frequency locking [1]. The simplest mechanism producing the OG signal is laser ionization of atoms or molecules, and in this context the technique is classified as a photoionization process. However, most OG investigations are based on weak cw laser excitation with a very low probability for the direct photoionization. A precise knowledge of the mechanisms leading to the OG effect under cw laser excitation is restricted to a few cases, mainly rare gas discharges. For instance, the OG effect in the positive column of a neon discharge has been interpreted by Doughty and Lawler [2] through a model where the ionization of the neon metastable levels by electron collisions play the dominant role.

Recently the OG and optoacoustic (OA) detections have been combined by us [3,4] in a low pressure rare gas discharge in order to obtain a more complete determination of the processes governing the discharge response under resonant laser excitation. The OA detection has proven that the laser light controls the amount of electrical power dissipated in the discharge, hence the temperature of the discharge itself. Depending on the discharge conditions, the laser light may produce a cooling or heating of the discharge [3].

In this paper we present a quantitative investigation of the change in the discharge dissipated power as a consequence of the laser irradiation of a neon positive column discharge. The optogalvanic and optoacoustic signals have been compared to the signals originated by a modulation of the discharge current. The measurements of the dissipated power have been compared to the Doughty and Lawler model [2] for the glow discharge.

The apparatus for the OG and OA detection is schematically represented in fig. 1. The OG detection scheme was based on the chopper modulation of a cw Rh-6G dye laser light and observation of the voltage modulation produced on the ballast resistor placed in series with the power supply. The OA detection was based on an electret microphone located near the anode, just outside the glow discharge region. The microphone detects the acoustic wave produced by the laser absorption in the discharge and

0 030-4018/88/$03.50

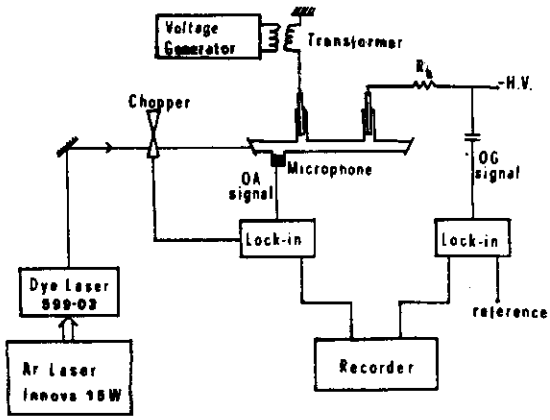

Fig. 1. Experimental apparatus for the OG, OA and EA detections.

the modification in the discharge temperature.

In order to probe the sensitivity of the microphone to the amount of power dissipated into discharge, a modulation of the discharge current, at the same frequency of the laser chopper, was applied through the transformer on the discharge circuit and the signal at the microphone was monitored. This so-called electro-acoustic (EA) signals, measured as a function of the discharge current and pressure, were used to analyze quantitatively the optoacoustic signals, as it will be presented in the following. A typical measured dependence of the EA signals on the discharge current is reported in fig. 2a.

OG and OA spectra obtained by laser irradiation of the neon positive column have been reported in previous papers [3,4] and will not be reported here. Briefly we have observed OG and OA signals whenever the dye laser frequency was in resonance with a neon transition from the metastable $1s_5$ and $1s_3$ levels, the quasi-metastable $1s_4$ level (owing to the radiation trapping) and the non-metastable $1s_2$ level to the $2p_j$ ($j=1,10$) levels. In the range of discharge currents explored in the experiment a typical spectrum reports negative OG signals associated to the transitions starting from the metastable levels, and positive OG signals associated to the transitions starting from other levels. The OA signals for the metastable level transitions may correspond to an increase or decrease of the discharge temperature. Figs. 3 and 2b report the dependence of the OG and OA signals respectively on the discharge current for laser

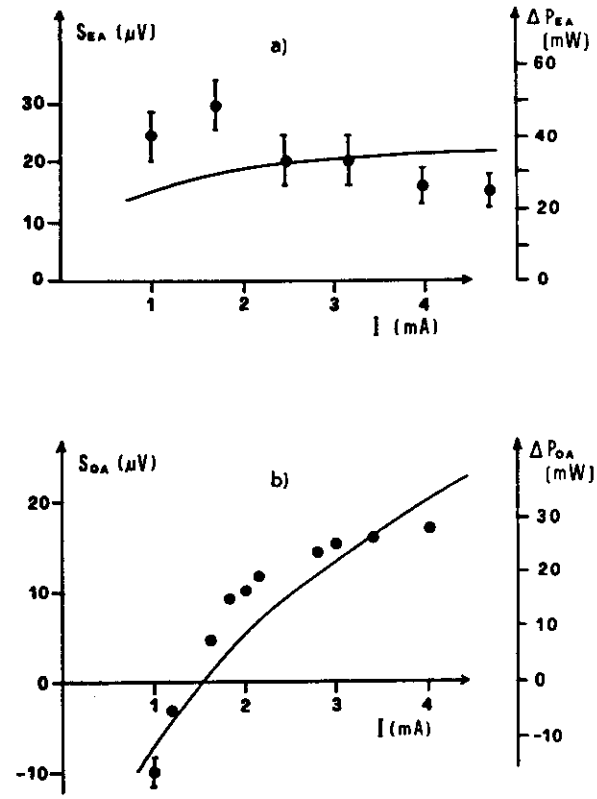

Fig. 2. Experimental results, with error bars, for the EA signals (a), and OA signals (b), versus the discharge current in a 1.5 Torr discharge. Theoretical curves for the internally dissipated power in the voltage modulation, $\Delta P(EA)$, and in the optoacoustic observations, $\Delta P(OA)$. Modulation voltage applied in the EA experiment was 5 V. Irradiation at 594.5 nm on the $1s_5$–$2p_4$ line was used in the OA observations.

irradiation on the 594.5 nm $1s_5$–$2p_4$ line of a 1.5 Torr neon positive column.

We have measured through a probe the electric field inside the positive column as a function of the current, and through atomic absorption the metastable density population and the translation temperature of the neon atoms (typically around 550 K). Finally the dynamic resistance of the discharge, i.e. the derivative of the discharge voltage drop in respect to the discharge current, was determined from the measured curve of the discharge voltage versus the current.

The current flow and the energy balance in the neon positive column are governed by the populations in the metastable levels. These levels are ion-

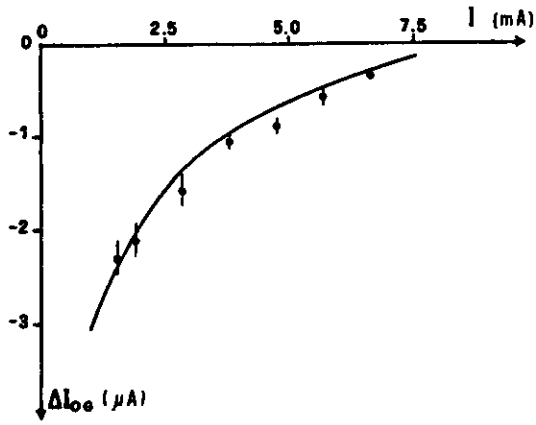

Fig. 3. Optogalvanic signals, with error bars, versus discharge current for the $1s_5$–$2p_4$ neon transition at 1.5 Torr pressure. The theoretical curves have been obtained from the model presented in ref. [2] as explained in the text.

ized through collisions with electrons or other neon atoms. Light absorption from the metastable levels to upper ones decreases the metastable level population and the discharge current flow.

The current I flowing through the discharge depends on the drift velocity v_d and the electron density n_e through the Tonks-Langmuir relation [5]

$$I=2\pi e r^2 h_0 v_d n_e , \tag{1}$$

where r is the discharge tube diameter and h_0 is a numerical constant taking into account the radial distribution of the electron temperature inside the discharge. The rate of change of the density M in the metastable $1s_5$ and $1s_3$ neon levels and in the quasi-metastable $1s_4$ level is governed by an equation including the production P for electron impact excitation from the ground state, the loss rate W by diffusion to the walls, the loss rate T for metastable-metastable associative ionization, the loss rate S for electron impact ionization and the loss rate $S'/4$ for electron impact excitation to the 2p levels,

$$dM/dt=Pn_eM-WM-TM^2 -Sn_eM-(S'/4)\,n_eM . \tag{2}$$

The rate of change of the electron density n_e is governed by production through α, the first Towsend coefficient, the impact ionization with rate S and the associative ionization of the metastables with rate T, and the loss by diffusion to the wall with the D_a ambipolar diffusion coefficient,

$$dn_e/dt=\alpha v_d n_e+Sn_eM +(T/2)M^2-D_a(2.4/r)^2 n_e . \tag{3}$$

The production and loss rate coefficients for the metastable and electron density were calculated in ref. [2]. The non-metastable $1s_2$ level R density is determined by the electron excitation from the ground state and from the metastable levels and by the decay rate w_2 for the ultraviolet emission. We estimated the R population by using the theoretical analyses of refs. [2,4] and a comparison to the M population.

Absorption of Q photons on the 594.5 nm neon line modifies the M and R densities. If $\beta=0.44$ is the branching ratio for decay to the $1s_2$ level, absorption of Q photons per unit time depletes the M population of eq. (2) by a βQ rate and fills the $1s_2$ population by the same rate. The modifications ΔM, ΔI_{OG} and Δn_e introduced by the laser absorption may be derived from a perturbation to the steady state solutions of eqs. (1)–(3), taking into account that (i) the electric field inside the discharge is modified by the laser irradiation; (ii) the drift velocity and the first Towsend coefficient depend on the electric field as shown in ref. [6]; (iii) the electric field variation is connected to the OG signal through the following relation:

$$L\Delta E=-R_b\Delta I_{OG} , \tag{4}$$

L being the positive column length, E the electric field and R_b the ballast resistor.

Determination of the discharge parameters appearing in eqs. (1)f–(3) and describing the unperturbed discharge would allow a derivation of the ΔI_{OG} signal from those equations. However as already done in refs. [2,5], we have chosen to obtain information on the unperturbed discharge through a determination of the dynamic resistance of the discharge. Thus only the parameters appearing in eq. (2) for the metastable balance are required to derive the amplitude of the ΔI_{OG} signal. Using parameters from ref. [2] and the measured dynamic resistance, we have obtained for the OG signal as a function of the current, the continuous line drawn in fig. 3, in very good agreement with the experimental results.

When the discharge current is modulated with a modulation amplitude ΔI_{EG}, as measured on the ballast resistor, under the application of a sinusoidal voltage V, the modification of the electron density becomes

$$\Delta n_e = \frac{n_e}{I}\left[\Delta I_{EG}\left(1+\frac{R_b}{L}\frac{I}{v_d}\frac{\delta v_d}{\delta E}\right)-\frac{1}{v_d}\frac{\delta v_d}{\delta E}\frac{V}{L}\right]. \quad (5)$$

This modification of the discharge originates the acoustic EA signals reported in fig. 2a.

The energy balance in the glow discharge illuminated by the laser beam at frequency ν includes as source terms the electric power $P_e = ILE$ and the light power $Qh\nu$. The input power is dissipated into different output channels: P_{vis} due to emission of neon visible fluorescent light transmitted by the cell walls; P_{uv} due to emission of neon ultraviolet fluorescent light on the $1s_{2,4}$–$1s_0$, transitions, followed by absorption of the radiation by the cell walls; P_{dif} the energy released by the deexcitation of the metastable atoms diffusing to the walls with rate W; P_{rec} the energy released by the electron–ion pairs migrating by ambipolar diffusion to the walls and recombining there; P_{co} due to conduction of heat to the walls by ground state neon atoms. Each energy term, except the last one, is related to the discharge parameters introduced in the eqs. (1)–(3). Their expression are the following ones [2].

$$P_{vis} = \pi r^2 LS' M n_e E_{vis} ,$$

$$P_{uv} = \pi r^2 LR w_2 E_R ,$$

$$P_{dif} = \pi r^2 LWME_M ,$$

$$P_{rec} = \pi r^2 LD_a (L/r)^{2.4} n_e^2 E_{ion} , \quad (6)$$

where E_{vis} is the average energy corresponding to the visible $1s_i$–$2p_j$ transitions; E_M and E_R are the energies of the metastable and quasi-metastable $1s_{3,5,4}$ and radiative $1s_2$ levels, respectively, and E_{ion} the neon ionization threshold.

We have verified that making use of the collision rates given in ref. [2] and the measured discharge parameters, in absence of laser irradiation the input electric power P_{el} is equal to the sum P_{tot} of the P_{vis}, P_{uv}, P_{dif}, P_{rec} powers dissipated into the different channels. This result is illustrated in fig. 4a as a function of the discharge current. As a consequence it appears that the power dissipated into the heat conduction by ground state atoms represents only a small contribution to the overall energy balance.

The laser absorption modifies the neon population and the energy balance. The determination of ΔM, ΔR and Δn_e allows to derive the variation ΔP_i of the above terms contributing to the energy balance of the positive column. The energy channels mainly perturbed by the laser radiation are the ultraviolet radiation emission ΔP_{uv} and the deexcitation of metastable atoms at the walls ΔP_{dif}, as shown in fig. 4b.

The acoustic signal monitors the change in the gas temperature, and the change in the discharge energy produced by the laser absorption could be connected to the OA signal through a determination of the temperature evolution inside the discharge. We have proceeded to a fit of the acoustic signals by supposing that the laser chopper modulation occurs at a frequency low enough to reach a stationary regime and that all the energy dissipated inside the discharge modifies the gas temperature. In the energy balance of the discharge the terms P_{uv}, P_{dif} and P_{rec} represent sources for the energy dissipation inside the discharge, whence should determine the gas temperature, while the energy released in the visible emission does not contribute to the gas temperature. The perturbation of those terms by the laser absorption should modulate the gas temperature and should represent the source of the acoustic signals. In fig. 2b the OA signal and the source for the acoustic signal, i.e. the variation of the internally dissipated power $\Delta P = \Delta P_{uv} + \Delta P_{dif} + \Delta P_r$, are compared as a function of the discharge current I. In fig. 2a we compare the EA signals and the variation of the internally dissipated power ΔP induced by the external voltage modulation V. In order to compare the vertical scales for the microphone signal and the power dissipated within the discharge, in figs. 2a and 2b one point of the theoretically evaluated ΔP power was fixed to an experimental point of acoustic signal and then the scale was fixed for both plots of fig. 2. The agreement between experimental and theoretical behaviors for the OA signal is very good and for the EA signal satisfactory. We attribute the remaining discrepancies to an incomplete transfer of the energy absorbed inside the cell to the gas temperature.

In conclusion the fit of the experimental results concerning the simultaneous galvanic and acoustic

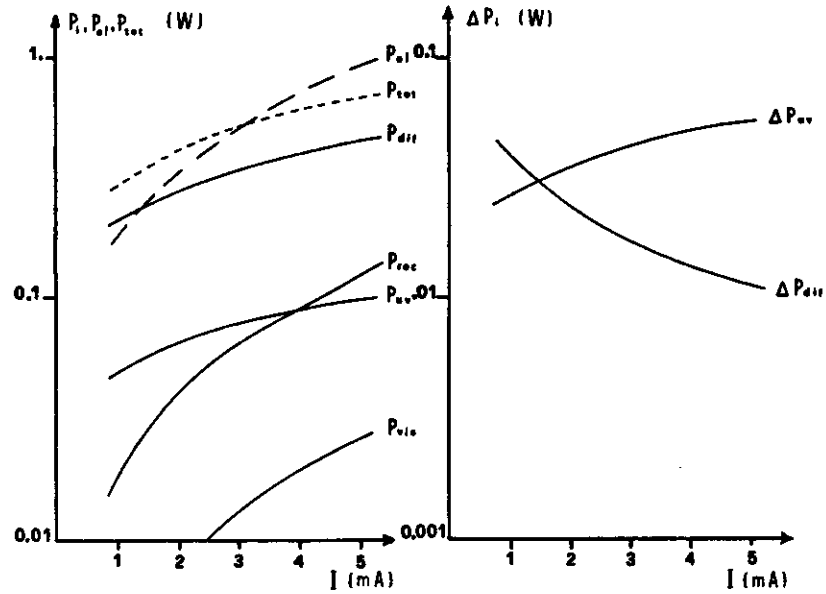

Fig. 4. Power balance of the positive column discharge as function of the discharge current I at the same pressure of fig. 2: (a) unperturbed energy balance; (b) laser perturbed energy balance.

detections proves that our analysis of the discharge perturbations and our knowledge of the discharge parameters are very good. The OG and OA detections represent techniques providing complementary information on the different mechanisms regulating a discharge under laser irradiation and may be used in combination to explore different discharges. A striking evidence of that complementary information is provided by the OA signal vanishing around 1.5 mA in the measurement of fig. 2b, while a non-zero OG signal is observed at the same current, as in the plot of fig. 3. That means that under particular conditions of the current discharge and gas pressure, no change of the dissipated power is induced by the laser radiation, even if the discharge current is modified by the laser absorption.

The financial support by the Ministero della Pubblica Istruzione through the Consorzio Italiano di Struttura della Materia is gratefully acknowledged.

References

[1] for a review, see Proc. Intern. Colloque on Optogalvanic spectroscopy and its applications, published in J. de Physique C7 (1983).
[2] D.K. Doughty and J.E. Lawler, Phys. Rev. A 28 (1983) 773.
[3] E. Arimondo, M.G. DiVito, K. Ernst and M. Inguscio, Optics Lett. 9 (1984) 530.
[4] A. Sasso, M. Ciocca and E. Arimondo, J. Opt. Soc. Am. B, to be published.
[5] J.E. Lawler, Phys. Rev. A 22 (1980) 1025.
[6] L. Tonks and I. Langmuir, Phys. Rev. 34 (1929) 876.
[7] J. Dutton, J. Phys. Chem. Ref. Data 4 (1975) 577.

Reprinted from Optics Letters, Vol. 9, page 530, December 1984

Laser cooling of a direct-current atomic discharge

E. Arimondo, M. G. Di Vito, and K. Ernst*

Istituto di Fisica Sperimentale, Università di Napoli, and Gruppo Nazionale di Struttura della Materia del Consiglio Nazionale delle Ricerche, 80125 Napoli, Italy

M. Inguscio

Dipartimento di Fisica, Università di Pisa, and Gruppo Nazionale di Struttura della Materia del Consiglio Nazionale delle Ricerche, 56100 Pisa, Italy

Received June 25, 1984; accepted September 19, 1984

Light-induced heating and cooling of a positive column discharge are demonstrated by combining the optogalvanic and optoacoustic detection. The phenomena that we have observed for laser radiation resonant with several Ne and He transitions are compared with a simplified energy model.

Absorption of resonant laser radiation induces changes in the electron density and the temperature of a discharge, resulting in the optogalvanic (OG) effect. The sensitivity of the OG technique, combined with excitation by means of high-spectral-purity tunable lasers, has permitted its application to high-resolution spectroscopy.[1] The change in the number of charged particles present in the discharge is believed to be the dominant process in the experimental observations of the normal atomic glow. However, significant features of the OG effect in molecular discharges[2] and in atomic hollow-cathode discharges[3] suggest that a modification in the temperature plays a significant role. In an experiment on a uranium hollow cathode, in which spectrally resolved fluorescent light was investigated, an increase in the discharge temperature was measured under resonant laser irradiation.[4] If a change in the discharge temperature is produced, we believed that the consequent acoustic disturbance could be detected by means of a microphone just as well as in the standard optoacoustic (OA) spectroscopy. We present in this Letter the first reported OA observation in a discharge. Combined OA and OG investigations were performed in He–Ne positive columns, for which a satisfactory quantitative model of the OG effect is available.[5,6]

Our apparatus was a standard positive column discharge in a glass tube of 0.25-cm radius and 21.5 cm long connected through a ballast resistor to a voltage-stabilized power supply. The aluminum electrodes were offset from the column axis. Pressures in the 50–500-Pa range and currents between 1 and 5 mA were used. The discharge tube was longitudinally irradiated with a cw Rh6G dye laser, whose beam was mechanically chopped at 310 Hz. The OG signal was detected across the ballast resistor. The acoustic waves were measured by two capacitive microphones: A microphone was placed on an outside wall of the discharge tube, while a second one inside the tube was placed near the grounded anode. The external microphone detected the acoustic disturbance directly generated by the ion-neutralizing collisions at the cathode. Owing to the OG current modulation, an acoustic wave at the chopper frequency was produced. The intensity of this wave followed the OG signal behavior, which was maximum near the cathode and negligible at the location of the internal microphone. The internal microphone detected the OA signals produced by the temperature changes in the discharge. Phase-sensitive detection was used, and OG and OA signals were recorded simultaneously while the frequency of the laser was scanned over the tuning range.

Typical spectra are shown in Fig. 1. OG and OA signals that are due to the He line at 587.6 nm and to several Ne transitions, exciting the metastable and nonmetastable levels of the $2p^5 3s$ configuration, have been investigated versus pressure and discharge current. Figure 2(a) shows the well-known dependence[6] of the

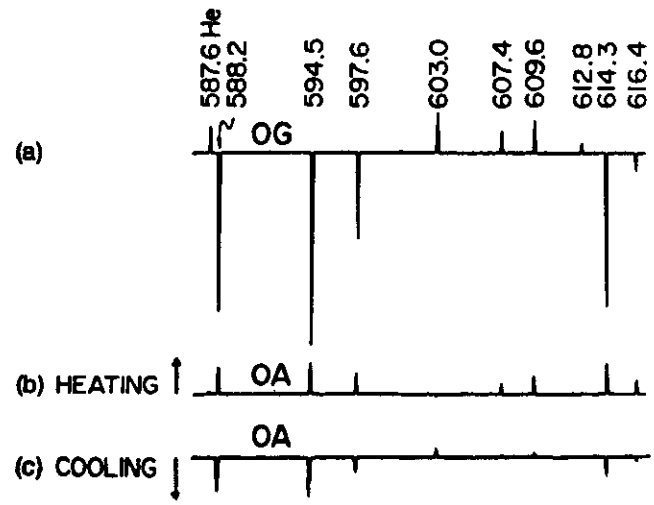

Fig. 1. Simultaneous two-pen recording of (a) the OG and (b) the internal-microphone OA signals in a He–Ne discharge (Ne, 133 Pa; He, 200 Pa) with a current i = 2.5 mA. Curve (c) is from a 399-Pa Ne discharge; i = 1 mA.

0146-9592/84/120530-03$2.00/0

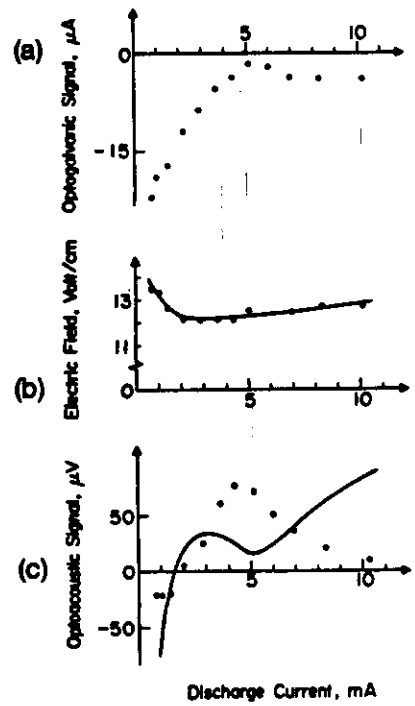

Fig. 2. Current dependence of the OG signal, the electric field E, and the OA signal, respectively, in the discharge of Figs. 1(a) and 1(b) under the 594.5-nm Ne line irradiation. The curve in (b) represents a best fit through the experimental points.

OG signal for the $1s_5$–$2p_4$ Ne line at 594.5 nm on the discharge current. Because the $2p_4$ level is radiatively connected to the ground state, the laser excitation at 594.5 nm depletes the metastable $1s_5$ level and produces the negative OG signal. A similar mechanism applies to all the Ne transitions starting from the metastable levels. Pressure and current dependences different from those of the OG signals were detected by the internal-microphone OA signal. This is shown in Fig. 2(c) for the current dependence of the 594.5-nm signal. Apart from a scaling factor proportional to the strength of the OG signal, the OA signals of all the Ne lines involving metastable levels presented the same current dependence. In fact, in Fig. 3(a) the current dependence of the OA signals for Ne lines starting from the $1s_5$ level is described by a single curve. A different OA behavior from that of Fig. 3(a) was exhibited by the 587.6-nm He line and all the Ne lines starting from the nonmetastable levels; however, they follow a similar scaling law, as is shown in Fig. 3(b).

Internal-microphone OA signals of opposite signs have been observed, which could not be directly ascribed to heating or cooling of the discharge. To clarify this point, a standard OA experiment, with the same cell arrangement as for the OG measurement with the discharge off, was performed in an absorbing molecular gas, in which the laser absorption definitely produces gas heating. From this observation we have deduced that the low-current OA signals of Fig. 2(c) correspond to discharge cooling and the high-current ones correspond to discharge heating. As a convention in Figs. 2 and 3 we have assumed that the positive OA signals correspond to discharge heating and the negative ones to discharge cooling. The microphone sensitivity was determined by producing a sinusoidal modulation of the discharge current by means of a transformer inserted into the power-supply circuit and by measuring the acoustic disturbance that occurred. Thus the largest negative OA signal shown in Fig. 2(c) was a cooling produced by a reduction of roughly 5 mW from the discharge. The current values of the maximum OA signal and of the zero OA signal of Figs. 2(c) and 3(a) depend on the discharge pressure and the ballast resistor. The different behavior observed in the OA signals at high currents in Figs. 2(c) and 3(c) was caused by different discharge electric fields.

The OA signal, i.e., the heating or cooling of the discharge gas, depends directly on the energy deposited into the gas and indirectly on the energy deposited at the discharge tube walls. The total input power is dissipated into the discharge through several channels: ionization, atomic collisional and radiative de-excitation, and heat conduction of ground-state atoms.[6] In the ionization channel the energy is ultimately released at the cell walls in the recombination process following the ambipolar diffusion of ions and electrons. In the collisional de-excitation channel the metastable atoms diffuse toward the walls, where they release their internal energy. In the atomic emission, the visible light is transmitted without absorption by the cell walls, while the vacuum-ultraviolet resonance radiation is absorbed. The contributions of the different channels to the discharge energy balance cannot be precisely determined, but they were estimated in Ref. 6 for a Ne positive column discharge in a glass tube with a radius comparable with that of the present experiment.

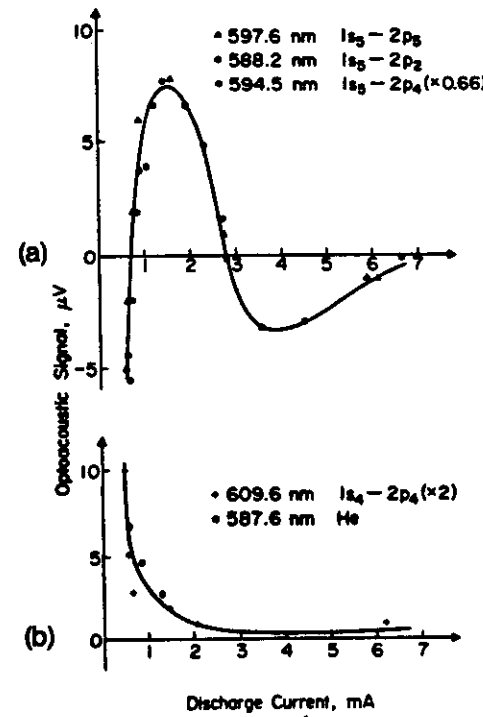

Fig. 3. Optoacoustic signals varying the discharge current for a He–Ne discharge (He, 200 Pa; Ne, 133 Pa).

Without laser irradiation of the discharge, a small fraction (5%) of the total electrical input power is lost in the emission of visible light. Another small fraction, less than a few percent of the total electrical input power, is lost in the heat conduction of ground-state atoms. The remaining input electrical power, lost in the vacuum-ultraviolet emission and in the wall recombination and de-excitation, is deposited into the discharge walls. Thus the major part of the input electrical power contributes directly or indirectly to the gas-discharge temperature.

The laser absorption modifies the atomic-population distribution and affects the power released into the cell through the different channels listed above. A precise analysis of the energy balance in the presence of the laser irradiation could give the dissipation in the power originating from the laser and producing the OA signal. Since this is not the case, we estimate the OA signal from the energy balance of the discharge. The input electrical power P_e is equal to lEi, where l is the positive column length, E is the axial electric field, and i is the discharge current. Under absorption of light power Q, the input electrical power is modified by a quantity δP_e. Most of the absorbed laser power Q is released from the discharge through the spontaneous emission of visible photons that are not absorbed by the cell walls and do not contribute to the discharge temperature. Thus only a small fraction f_L of the Q power contributes to the OA signal. Taking into account that the spontaneous-emission rate is larger than the rates for the electron-impact excitation to other levels and for the ionization, f_L could range between 10^{-2} and 10^{-3}. In an analogous way we defined by f_e the fraction of the electrical input power dissipated into the discharge temperature. From the analysis of the energy-dissipation channels, we have estimated that $f_e \simeq 0.9$–0.95. Thus we write that the OA signal is proportional to the change in the dissipated power ΔP given by

$$\Delta P = f_e \delta P_e + f_L Q = f_e l \delta(iE) + f_L Q = f_e(lE - Zi)\Delta i + f_L Q. \quad (1)$$

The last equality results because both i and E are modified under light illumination. Because a constant-voltage power supply was used, $l\Delta E = -Z\Delta i$. We have compared the results of our experiment with Eq. (1) using the current change measured in the OG effect, the discharge electric field E [Fig. 2(b)], and the absorbed power (between 0 and 13 mW) measured by means of a thermopile. According to the Q measurement and the f_L estimate, the light-power contribution is negligible in Eq. (1). A plot of Eq. (1) with $f_e = 1$ and $f_L = 0$ is represented by the continuous line in Fig. 2(c). The low-current experimental behavior is reproduced well. In particular, the low P_e term of Eq. (1) passes through zero at $i_n = lE/Z$, in agreement with the experimental result. At large current values a divergence between the behavior predicted by the δP_e term and the experimental observations arises, and a cooling process should be added to the energy balance of Eq. (1). A similar disagreement exists for the OA observations for the He and Ne nonmetastable lines, regardless of the current. These discrepancies come from the current-dependent f_e factor and the influence of the neglected absorbed laser-light term in Eq. (1). Moreover, at high currents, where the saturation of the metastable levels occurs, the available OG model is no longer valid.

The above results show that our understanding of the energy balance of a discharge is far from being complete. A deeper insight into the gas and wall energy deposit and the acoustic-wave production in such a weakly ionized plasma is required. However, from the analysis of the available experimental results, several conclusions can be derived: (1) Absorbed photons act as a switch controlling the electrical input power entering the discharge. Depending on the discharge conditions, an increase or decrease of the electrical power may arise, with a consequent heating or cooling. For instance, the latter may occur when the population distribution is modified by the laser absorption in such a way that the energy delivered at the walls by the ion recombination or the metastable de-excitation is smaller than that without the laser. Since the electrical power dissipated into the discharge is about 500 mW, the maximum 5-mW energy decrease in the experimental observations of Fig. 2(c) corresponds to a discharge temperature cooling of about 1%. (2) Equation (1) explains adequately the unified behavior of the metastable level OA signals in Fig. 3(a). The δP_e term is scaled by an amount Δi of the OG signal, and the absorbed light term, which depends mainly on the metastable population, has the same behavior for all the metastable lines examined.

In summary, this experiment suggests that under light illumination a direct compensation between electrical and laser powers may occur. The two terms in Eq. (1) can partially cancel each other, yielding positive, negative, and null contributions to the generated heat. In particular, direct evidence is given that under appropriate conditions a cooling of the laser-irradiated discharge may arise.

The authors are grateful to M. Allegrini, J. Hall, and J. Lawler for useful discussions and a critical reading of the manuscript.

* Permanent address, Institute of Experimental Physics, University of Warsaw, Warsaw, Poland.

References

1. J. F. Lawler, A. I. Ferguson, J. E. M. Goldsmith, D. J. Jackson, and A. L. Schawlow, Phys. Rev. Lett. 42, 1046 (1979).
2. C. R. Webster and R. T. Menzies, J. Chem. Phys. 78, 2121 (1983), and references therein; R. F. Muenchausen, D. May, and G. W. Hills, Opt. Commun. 48, 317 (1984).
3. R. A. Keller, B. E. Warner, E. F. Zalewski, P. Dyer, R. Engleman, Jr., and B. A. Palmer, J. Phys. (Paris) 44, C7-23 (1983), and references therein.
4. C. Dreze, Y. Demers, and J. M. Gagne, J. Opt. Soc. Am. 72, 912 (1982).
5. J. E. Lawler, Phys. Rev. A 22, 1025 (1980).
6. D. K. Doughty and J. E. Lawler, Phys. Rev. A 28, 773 (1983).

OPTOACOUSTIC INVESTIGATION OF THE MECHANISMS IN THE INFRARED OPTOGALVANIC EFFECT

C. HAMEAU, E. ARIMONDO [1], J. WASCAT and P. GLORIEUX
Laboratoire de Spectroscopie Hertzienne associé au C.N.R.S., Université de Lille I, 59655 Villeneuve d'Ascq Cedex, France

Received 15 November 1984

Simultaneous observations of the optogalvanic and optoacoustic effects were performed in CO_2, NH_3 and SF_6 discharges under irradiation by resonant infrared 10 μm laser radiation. The dependence of the galvanic and acoustic signals on the discharge current, and their time evolution following a switch of the laser radiation were investigated. The observations proved that the infrared optogalvanic effect occurs through two different mechanisms, a gas kinetic temperature dependence of the discharge parameters and a modification of the pion production through the vibrational molecular excitation.

1. Introduction

In the laser optogalvanic (OG) effect the current flowing through an atomic or molecular discharge is monitored, while a laser irradiation on an atomic or molecular transition occurs. In atomic spectroscopy on transitions involving visible radiation, the main mechanism leading to the OG effect is the dependence on the atomic excitation for the processes of ion production, for instance the associative ionisation and the electron impact ionisation [1]. However in the atomic hollow cathode discharges an increase in the electron and gas temperatures produced by the collisions with excited atoms was invoked in the analysis of the OG effect [2]. Observations of the OG effect on infrared transitions between highly excited atomic levels [3] and between vibrational molecular levels [4–8] have shown that the impedance of a discharge may be modified also by the absorption of small energy infrared photons. Webster and Menzies [6] suggested that for the vibrational molecular transitions, where the electronic state is not modified in the absorption, the OG effect arises through an heating mechanism. The absorbed laser energy is converted into a gas temperature increase through the vibro–translational (V–T) relaxation process. The change in the current flowing through the discharge should arise from the temperature dependence of a relevant discharge parameter, for instance either the electron impact ionisation, or the electron attachment or the electron-ion recombination. This interpretation of the molecular OG effect was supported by the time resolved experiments with pulsed laser excitation, where it was shown that for a laser absorption outside the discharge region, the OG effect was produced by the propagation of a thermal acoustic wave through the gas [5,7].

The direct observation of the energy deposited into the discharge by means of the optoacoustic (OA) effect may provide additional information on the mechanisms producing the OG effect. Thus, as done previously in atomic discharges [9] we made simultaneous observations of the OG and OA effects for infrared vibrational excitation of molecular CO_2, NH_3 and SF_6 discharges.

Depending on the discharge operating conditions and on the position of the laser irradiation, the OG and OA signals presented a similar or different behaviour. Thus the OG effect should proceed through two different mechanisms. The behaviour of a molecular discharge at low fractional ionization values is governed by the

[1] Permenent address: Istituto di Fisica Sperimentale Università di Napoli, Italy.

0 030-4018/85/$03.30

electron kinetic processes (i.e. the ionization, the attachment and the recombination occurring in the electron collisions with molecules and ions), the transport processes (electron and ion drift and diffusion) and the relaxation processes determining the gas heating. Because the laser radiation induces a population transfer between the vibrational levels, the dependence of the electron kinetic processes on the vibrational state may play an important role in producing the OG effect.

The kinetic and transport processes are also a function of the gas translational temperature. The vibrational laser excitation is converted into a gas heating increase through the relaxation processes and this translational temperature increase modifies the current flow.

2. Experimental apparatus

The optogalvanic set-up, similar to that used in refs. [6] and [8] was composed by a glass cell, 1.2 cm internal diameter, containing an hollow cathode and a rod or ring anode, all made of stainless steel. The cell electrodes were mounted on sliding connections in such way that the interelectrode separation and the region of the laser excitation could be modified in the 0.5–9 cm range. The laser radiation, coming from CO_2 or N_2O flowing gas lasers and focused to a 2 mm radius spot at the cell center, was coupled perpendicularly to the discharge cell axis through ZnSe Brewster windows mounted on two transverse arms. The discharge cell was operated in the normal glow regime either sealed off or with a gentle flow of gas maintained through.

The OG signal was measured across a 200 Ω series resistor. A condenser microphone with an internal FET amplifier was mounted on the cell transverse arm, halfway between the cell center and one ZnSe window.

3. Results

3.1. CO_2

A positive OG signal, i.e. an increase in the current i flowing through the discharge, was observed under irradiation by CO_2 laser light. Observations at different laser lines, laser powers, irradiation positions inside the discharge, CO_2 flowing rate and discharge currents were performed. Fig. 1 reports the temporal dependence of the OG and OA signals at laser switch-on and switch-off. The signals were obtained in a 5 cm length discharge, with 10 P(20) laser irradiation inside the positive column, at a constant discharge current and different CO_2 pressures. The OA signals had the shape typical of a microphone detection system with the gas flowing through the OA cell [10]. In the central part of the 7 ms laser pulse they presented a slowly varying component limited mainly by the time constant of the thermal diffusion towards the cell walls. This diffusion component appeared very clearly in the 10 mbar measurements, where a large laser energy was deposited into the cell. The initial and final transient acoustic signals exhibited a periodic structure with a time period independent of the gas pressure and of the

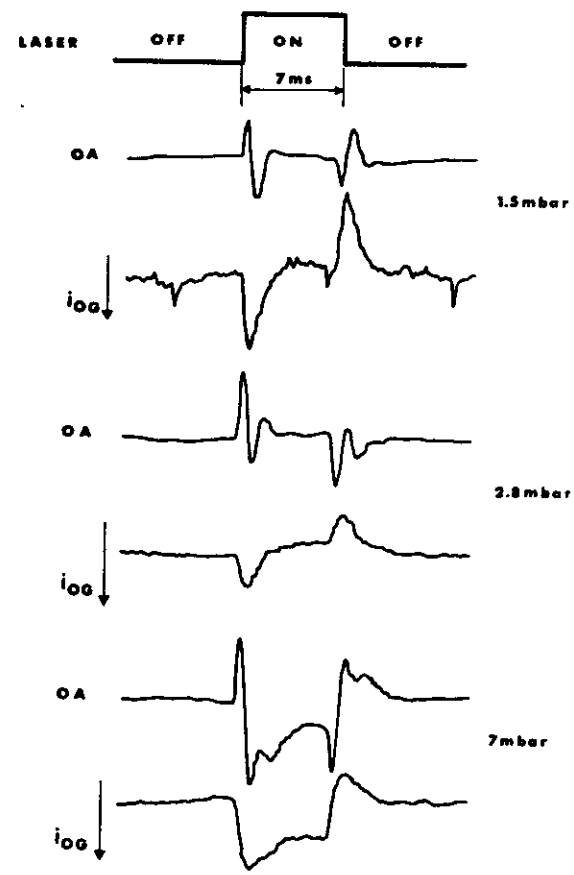

Fig. 1. Time evolution of the OA signals (upper records) and of the OG signals (lower records) for 2 W 10 P(20) laser irradiation inside the positive column of a 14 mA, CO_2 discharge.

laser intensity. That structure was originated by acoustic resonances in the cell or the microphone. A striking result from the photos of fig. 1 is that the OA and OG signals presented a very similar temporal behaviour, thus proving in a direct way for the CO_2 molecules the OG signals are produced by the translational temperature increase detected by the OA microphone.

Whichever the position of the laser irradiation inside the positive column, the transient and slowly-varying OA and OG signals presented the typical behaviour of fig. 1. On the contrary a negative OG signal appeared when the laser illuminated a region on the back of the anode outside the discharge. In these conditions the transient OG signal resulted very small; the slowly varying component was not reduced in amplitude and appeared with an inverted sign.

By applying a 400 Hz modulation of the laser radiation and phase sensitive detection an investigation of the amplitude for the OG and OA signals versus the discharge current was performed, as reported in fig. 2. A 5 cm CO_2 discharge was irradiated in the central part of the positive column by 4 W 9P (12) CO_2 laser radiation. Similar results were obtained at different discharge pressures and laser irradiation positions both in the positive column and on the back of the anode electrode. The OG signals depended on the CO_2 flow rate through the cell, as shown in fig. 2. The OG effect

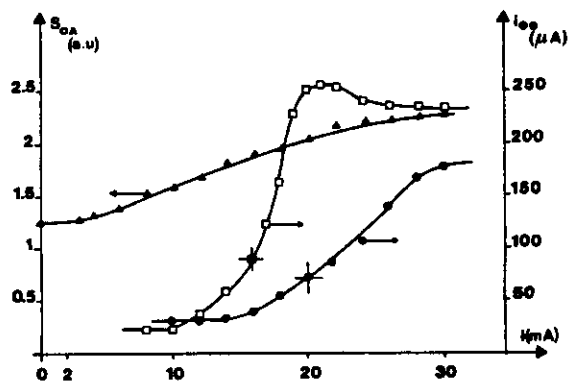

Fig. 2. Amplitude of the OG signals versus the current i and of the OA signals for a 11 mbar CO_2 discharge under irradiation by 10 P(22) CO_2 laser line. The ○ and ● points of the OG signal were obtained respectively at medium and low flow rate through the discharge cell. The lines passing through the experimental points have been drawn for convenience of presentation only.

presented a maximum in the current explored range and the current of the maximum shifted to a lower value by reducing the CO_2 flow rate.

In the OA results of fig. 2 a large signal appeared when the discharge did not operate. The OA signal increased in amplitude when the discharge was switched on and the current was raised to 30 mA, whichever the CO_2 flow rate in the cell. This dependence of the OA signal on the discharge current arised from an increase in the number of absorbing molecules when the discharge was on. Vibro–rotational temperatures in the 400–500 K range are typically reached inside a CO_2 discharge, and such a temperature increase explains quantitatively the two times increase in the absorption coefficient, whence in the OA signal, observed for the discharge current rise from 0 to 30 mA.

3.2. NH_3

For the OG and OA studies in ammonia discharges, we used the 1.3 watt power radiation from an N_2O laser operating on the P(13) line, for which the ammonia gas has a strong absorption coefficient. Thus large OG and OA signals were observed for discharges runnning at a maximum 2 mbar pressure, lower than that typically used in the CO_2 discharges. Fig. 3 reports the time evolution of typical OA and OG signals obtained under different discharge conditions. Fig. 3a represents the OA signal observed at the switches on and off of the laser radiation on a 0.3 mbar discharge, and similar results were obtained on discharges at different ammonia pressures. The time dependence of the OA signal is very similar to that observed in the CO_2 discharges with the transient and slowly varying acoustic signals, except that the transient structures produced by the acoustic resonances were not observed in the low pressure range. The OG signals of figs. 3b–d were obtained for laser irradiation inside the positive column at different currents and pressures, while the OG signal of the (e) photo was obtained for irradiation near the cathode in the negative glow region. An increase in the discharge current (positive OG signal) was produced for irradiating anywhere inside the positive glow, and a decrease in the discharge current (negative OG signal) resulted from irradiation in the negative glow. Fig. 4 reports this behaviour of the OG signal as function of the irradiation position inside the cell under gentle gas flow conditions. It may

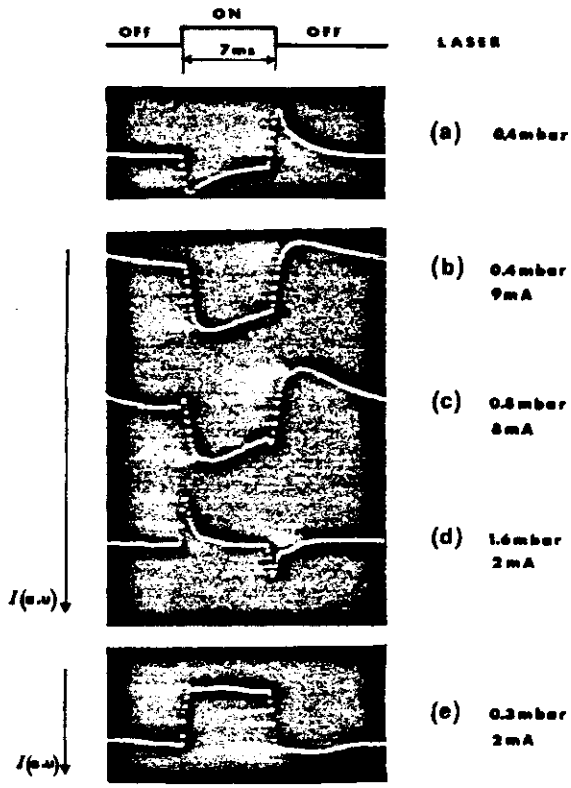

Fig. 3. Waveforms of the OA and OG signals for the P(13) N_2O laser irradiation of a NH_3 discharge. A typical OA signal is represented by the a photo. The (b)–(d) OG signals resulted for irradiation inside the possitive glow of the discharge. The (e) negative OG signal was obtained for irradiation inside the negative glow.

be noticed that the change from positive to negative OG signals occured in a very small region at the beginning of the negative glow. The determination of this region was limited by the laser beam diameter. Fig. 4 represents the spatial dependence of the ammonia OG signal which was qualitatively described in ref. [6]. Figs. 3b–d present the modifications originated in the positive glow OG signal by an increase in the ammonia pressure. At low pressure the OG signal was positive during all the laser pulse, with a signal risetime equal to that observed in the OA signal. Increasing the ammonia pressure a negative transient signal appeared at the laser switches on and off. Thus in the (d) record at 1.5 mbar pressure the positive glow OG signal was composed by a large negative transient signal with some structure inside.

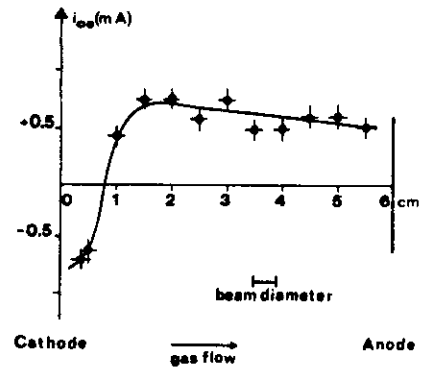

Fig. 4. Amplitude of the OG current signal versus the discharge irradiation positions for 0.5 mbar NH_3 pressure at 2 mA current. The line through the points has been drawn for convenience only.

From an investigation of the risetime in the OA and OG waveforms, the OG signal appeared delayed with respect to the laser absorption measured by the OA signal. The delay time increased with the distance of the irradiation position from the cathode. For instance at a 0.4 mbar pressure, 2 mA current in a 7.5 cm discharge and irradiation at 7 cm from the cathode the initial rise of the OG signal appeared delayed by 0.3 ms with respect to the laser absorption.

3.3. SF_6

Very strong OA signals were observed in SF_6 discharge under irradiation by the 10P (24) CO_2 laser line. Very weak positive OG signals were obtained within a limited range of discharge operation, for instance at 1 mbar pressure and 1 mA current. The OA and OG waveforms presented a similar temporal dependence, as in the CO_2 discharge.

4. Discussion

The similarity of the OA and OG waveforms in the CO_2 and SF_6 discharges confirms the existence of one phenomenon producing both the acoustic and galvanic effects. On the contrary in NH_3 several phenomena simultaneously contribute to the later, so that different waveforms were observed in the two effects. The OA signal originates from an increase in the gas translational temperature through the roto-translational

R–T and V–T relaxations. The change in the current flow in the discharge should depend on this translational temperature increase. The kinetic and transport discharge processes depend also on the vibrational temperature of the molecular and if the laser modifies this temperature, the electrical conduction of the discharge will be modified. In the cases where the laser induced change in the translational temperature is the dominant phenomenon in controlling the discharge current, the observed OA and OG waveforms have a similar time evolution, because the time delays introduced by the electron–molecule collisions and the acoustic wave propagation are negligible on the time scale of the chopper modulation. Such a behaviour applied to the CO_2 and SF_6 observations. In the cases where the laser induced change in the vibrational temperature is important in determining the current flow, the time evolution of the OG signal is governed by the slow V–T relaxation time (typically in the ms range). This behaviour occurred in the NH_3 discharge.

To provide a complete description of the OG effect, the molecular processes where the changes in the translational or vibrational temperatures play the dominant role should be determined, but the knowledge of the discharge molecular phenomena is not precise enough. For the time being, we can only describe schematically the overall mechanism of the OG effect through the block diagram of fig. 5 and list some relevant discharge processes modified by the laser absorption.

The translational gas temperature appears in the discharge energy balance through the energy delivered

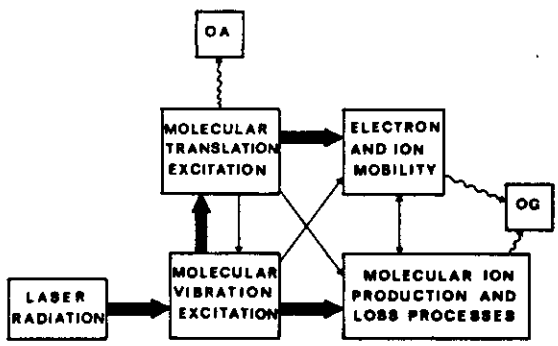

Fig. 5. Block diagram of the infrared OA and OG effects in molecular discharges. The main processes discussed in the text are represented by the bold arrows. Additional processes contributing to the discharge equilibrium are also represented.

in the elastic collisions of the electrons and ions with the molecules. Thus the electron and ion mobilities may depend on the translational gas temperature. A theoretical investigation of the electron collisions showed that the electron mobility and the electron characteristic energy in the CO_2 gas are temperature independent, while in the NH_3 gas they are a strong function of the gas temperature [11]. Thus the temperature dependence in the electron collision is certainly an important mechanism in the OG effect in NH_3, while the CO_2 gas behaviour requires a further investigation. The gas temperature dependence of the ionic mobility could be another important parameter controlling the discharge conductance. It should be noticed that the time delay reported for the NH_3 OG signal with respect to the OA signal may be interpreted as an acoustic disturbance propagating through the discharge from the laser irradiation region to the negative glow near the cathode. In the negative glow a large concentration of positive ions is present, and a change in the ionic mobility is relevant for the current flow.

The molecular distribution over the vibrational states, whence the vibrational temperature affects the formation of negative and positive ions in the electron–molecule collision. In the CO_2 and NH_3 discharges the positive ions are produced by electron impact ionization and the negative ions by dissociative attachment, however the dissociation attachment cross-section in NH_3 is ten times larger than in CO_2 and varies considerably with the electron energy [12]. In CO_2 and SF_6 that cross-section increases by one order of magnitude at maximum for a molecular excitation to vibrational excited levels [13] similar data are not available for ammonia but a vibrational increase of the cross-section may explain the OG negative signals, i.e. the decrease in the discharge current, for molecular excitation to the upper vibrational level. It should be also considered that owing to the multiphoton laser absorption or the resonant vibration–vibration energy transfers, the excitation of molecules to highly excited vibrational levels may be produced.

An analysis of the infrared OG effect in atomic discharges [1,3] stated that the change i_{OG} in the discharge current is equal to the number of absorbed photons multiplied by the efficiency in the ionization mechanism and by the efficiency in the ion and electron collection. This collection efficiency is derived from the voltage current characteristics of the dis-

charge and the OA signal measures directly the absorbed photons. From the results presented in fig. 2 it turned out that the efficiency in the ionisation mechanism was a function of the current. That showed that even if in the CO_2 discharges the OG effect arises from the kinetic gas temperature increase produced by the absorbed power, the ionization mechanism leading to the OG effect is a function of the current, i.e. the electron and ion densities. Our OG dependence on the discharge current is anomalous in comparison to a previous OG analysis inside a CO_2 laser [14], where the largest OG signal appeared at low discharge currents. We observed such an OG behaviour only in a sealed discharge cell for irradiation on the back of the anode.

An important difference appears between the OG effects in atomic and molecular discharges when their laser absorbed power and electric power change are compared. On the basis of the CO_2 absorption coefficient the absorbed power in the conditions of fig. 2 resulted approximatively 200 mW and the electric power change a few milliwatts. On the contrary in the atomic discharges the net laser absorbed power was typically smaller than the electric power change [9]. In the atomic discharges the laser radiation controls the dissipated electric power and the change in the electric power leads to a modification of the gas temperature in the discharges whence the OA effect. On the contrary in the molecular discharges the change in the gas temperature is produced by the laser absorbed power dissipated through the relaxation mechanisms, and the gas temperature increase produces the OG effect and the electric power changes.

In conclusion the simultaneous observation of the infrared OA and OG effects has shown that the dissipation of the absorbed power into the R–T and V–T relaxation leads to the OG effect. The increases in both the kinetic gas temperature and the vibrational temperature affect the discharge current through independent processes. The positive and negative molecular OG signals observed in the present investigation as well in another [6] are connected on the influences of the kinetic gas temperature and of the vibrational temperature respectively. The mobility, ionisation, attachment and recombination processes precisely modified by a temperature increase cannot be specified because of the incomplete knowledge of the molecular discharge chemistry. Further investigation on these electron–molecular collisional processes is required to set up a rate equation model providing a quantitative comparison with the observed signals.

Acknowledgment

One of the authors (E.A.) wishes to thank R.J. Hall for a discussion on the measurements of the dissociative ionization cross-sections.

References

[1] J.E. Lawler, Phys. Rev. 22A (1980) 1025;
D.K. Doughty and J.E. Lawler, Phys. Rev. 28A (1983) 773.
[2] R.A. Keller, B.E. Warner, E.F. Zalewski, P. Dyer, R. Engleman Jr. and B.A. Palmer, J. Physique 44 (1983) 23.
[3] D.J. Jackson, E. Arimondo, J.E. Lawler and T.W. Hansch, Optics Comm. 33 (1980) 51;
H. Bergemann and R.J. Saykally, Optics Comm. 40 (1982) 277.
[4] A.I. Carswell and J.J. Wood, J. Appl. Phys. 38 (1967) 3028.
[5] C.T. Rettner, C.R. Webster and R.N. Zare, J. Phys. Chem. 85 (1981) 1105;
D.A. Haner, C.R. Webster, P.H. Flamant and I.S. McDermid, Chem. Phys. Lett. 96 (1983) 302.
[6] C.R. Webster and R.T. Menzies, J. Chem. Phys. 78 (1983) 2121.
[7] R.E. Muenchausen, R.D. May and G.W. Hills, Optics Comm. 48 (1983) 317.
[8] C. Hameau, J. Wascat, D. Dangoisse and P. Glorieux, Optics Comm. 49 (1984) 423.
[9] E. Arimondo, M.G. Di Vito, K. Ernst and M. Inguscio, J. Physique 44 (1983) 267; Optics Lett. (1984), to be published.
[10] L.R. Rosengreen, E. Max and S.T. Eng, J. Phys. E. Sci. Instr. 7 (1974) 125.
[11] J.L. Pack, R.E. Vorshall and A.V. Phelps, Phys. Rev. 127 (1962) 2084;
R.D. Hake Jr. and A.V. Phelps, Phys. Rev. 158 (1967) 70.
[12] V.A. Bailey and W.E. Duncanson, Phil. Mag. 10 (1930) 145;
T.E. Sharp and J.T. Dowell, J. Chem. Phys. 50 (1969) 3024.
[13] P.J. Chantry, J. Chem. Phys. 57 (1972) 3180;
C.L. Chen and P.J. Chantry, J. Chem. Phys. 71 (1979) 3897.

Optogalvanic investigations in the cathodic region of a neon glow discharge

E. DeMarinis and A. Sasso[a)]
Dipartimento di Fisica N.S.M.F.A., Universitá di Napoli, Mostra d'Oltremare, Pad. 20, 80125 Napoli, Italy

E. Arimondo[a)]
Dipartimento di Fisica, Universitá di Pisa, Piazza Torricelli, 2, 56100 Pisa, Italy

(Received 11 March 1987; accepted for publication 9 September 1987)

We report on an investigation of the optogalvanic effect in the cathodic region of a glow discharge. Analysis of the spatial behavior of the fluorescence intensity enabled us to obtain detailed information on the laser-unperturbed discharge. A description of the discharge maintenance mechanisms through the secondary electron emission from the cathodic surface by the impact of ions, metastable atoms, and VUV photons has been used to describe the current-voltage tube discharge characteristics. The laser-induced perturbation of the secondary emission has been understood as the main mechanism responsible for optogalvanic production in our discharge configuration.

I. INTRODUCTION

In recent years the optogalvanic (OG) effect has been shown to be a powerful technique for several spectroscopic studies and analytical determinations.[1] The aim of many investigations, made with different experimental conditions, has been to understand the mechanisms which regulate the OG signal production.[2–4] A deeper comprehension of the OG processes is relevant for improving the OG detection sensitivity. Moreover, the main processes governing weak plasmas may be isolated through the study of the OG mechanisms. Nevertheless, a complete knowledge of these mechanisms is restricted to very few cases. In particular, an analysis of the sign of the neon positive column OG signals as a function of laser power, discharge current, and neon pressure has been described in Ref. 5. Later, Doughty and Lawler[6] developed a quantitative model which describes well the optogalvanic signals induced by laser radiation resonant with $1s \rightarrow 2p$ neon transitions (Paschen notation).

In that model, positive (current increase) or negative (current decrease) OG signals were explained on the basis of changes in the density of metastable levels ($1s_{5,3}$) which play an important role in the following multistep ionization electron impact processes:

$$\mathrm{Ne}(1s_i) + e^- \rightarrow \mathrm{Ne}^+ + 2e^-, \quad i = 5,3. \tag{1}$$

When a transition from a metastable level is laser induced, the electron density maintained by process (1) is decreased owing to a depletion of the metastable density. On the other side the electron density is increased when a radiative level ($1s_{4,2}$) is depleted by laser radiation. In fact, radiative decay down to the metastable levels following the $1s_{4,2} \rightarrow 2p$ laser excitation increases the efficiency of process (1). In contrast to the positive column, where reasonable modeling of the discharge exists,[7] the knowledge is more empirical for other regions of a glow discharges such as the cathodic region.

In this paper we present an investigation of the OG effect near the cathodic surface of a neon discharge with two plane parallel electrodes. In this discharge configuration the mechanisms of electronic emission from the cathodic surface produced by the impact of ions, metastable atoms, and photons play a key role in sustaining the discharge. When resonant radiation interacts directly or indirectly with ions or metastables, the electrical conduction properties of the discharge are strongly modified. In the positive column experiments, the electrodes are offset from the column axis to avoid interaction between the incident laser beam and the area near the cathodic surface. In this way the laser perturbation does not act directly on the electron emission at the cathodic surface.

Our experimental work has been organized as follows: A preliminary analysis of the discharge fluorescence permitted us to characterize the principal parameters of the discharge in terms of the dark-space extension. The metastable atom density is measured by a standard absorption technique. By using a tunable dye laser many of the $1s \rightarrow 2p$ neon transitions have been investigated using the optogalvanic effect. In particular, a spatial analysis of the OG signal has been made. Our results show that the OG signals in the cathodic region are explained through a variation of the secondary electron emission from the cathode surface. This mechanism is dominant compared to the direct current variation induced by the neon multistep ionization.

Our description of OG processes is based on a balanced equations approach for electron and ion currents. In the hypothesis of small OG signals the perturbed equations give an analytical expression of the current change ΔI in terms of the more significant parameters of the discharge. Our model is also relevant to other discharges where the secondary electron production has a key role, as, for instance, in the hollow cathode discharge.

II. THEORY

The cathodic part of the glow discharge is divided into the Crookes dark space, the negative glow, and the Faraday dark space. The last region does not have a significant role,

[a)] Also at Centro Interuniversitario di Struttura della Materia, Italy.

 0021-8979/88/030649-07$02.40

both for fluorescence and optogalvanic signals, due to low excitation of the atomic or molecular species, and for this reason it will not be considered in our model.

In contrast to the positive column, the cathodic region is characterized by nonhomogeneous electrical properties. The electric field, created by the voltage difference across the electrodes, is large at the cathodic surface and drops almost to zero in the few millimeters of the dark-space extension.

The electons near the cathode surface are strongly accelerated by the electric field of the Crookes space, where very few inelastic collisions with neon atoms take place. When the electrons enter into the negative glow, a swarmlike motion begins and several inelastic and ionization processes occur. These collisions lead to an abrupt growth of fluorescence at the negative glow wedge. The electron-impact excitation of the radiative $1s_4$ and $1s_2$ neon levels is followed by emission of VUV photons at 743.7 and 735.9 Å, respectively. The metastable atoms, ions, and VUV photons produced by primary electron collisions are collected, with different efficiencies, by the cathode surface and produce the secondary electrons. Following the OG neon description introduced by Doughty and Lawler,[6] the $1s_5$ and $1s_3$ levels are lumped together as a single metastable level with total density population $\mathscr{M}$. The density population of the radiative $1s_4$ and $1s_2$ levels will be denoted in the following by $\mathscr{R}$.

The total current density $J(x)$ at a distance x from the cathode surface (see Fig. 1) contains a contribution from ions (J^+) and electrons (J^-):

$$J(x) = J^+(x) + J^-(x). \tag{1}$$

At the cathode surface ($x = 0$) the electron density current may be expressed as

$$J^-(0) = \gamma_i J_i(0) + e\gamma_m J_m(0) + \gamma_p [J_d(0) + J_g(0)], \tag{2}$$

where γ_i, γ_m, and γ_p are the efficiencies of the secondary electron emission from the cathode surface for the impact of ions, metastable atoms, and photons, respectively.

With respect to the theory developed in Ref. 7, in Eq. (2) we have explicitly taken into account the contribution of the impact of metastable atoms to the secondary emission.[8] The transport of metastable atoms to the cathode is regulated by a diffusion process. The flux density of the metastable atoms on the cathode surface is given by

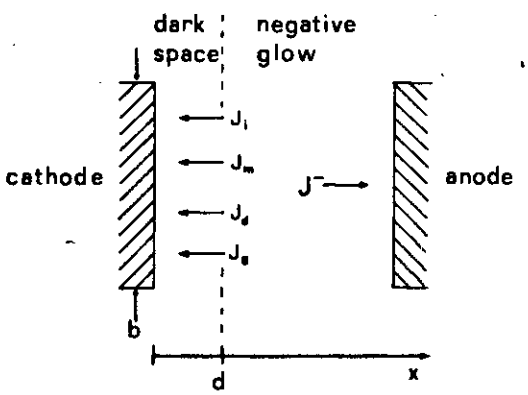

FIG. 1. Scheme of the secondary electron emission from the cathode surface.

$$J_m(0) = D_m \frac{\partial \mathscr{M}}{\partial x}(x)\Big|_{x=0}, \tag{3}$$

where D_m is the diffusion coefficient.

We assume the spatial distribution of metastable atoms to be[9]

$$\mathscr{M}(x) = 0, \quad x < x_m,$$
$$\mathscr{M}(x) \propto \exp[\alpha(x - x)], \quad x < x < d, \tag{4}$$

where x_m is the distance which an electron must traverse in the direction of the field to obtain the energy of excitation of the metastable state; α is the first Townsend coefficient.

We may write the flux density in the following form:

$$J_m(0) = \alpha D_m \exp(-\alpha x^*)(x), \tag{5}$$

x^* being the distance from the cathode where the metastable density has been measured. In our experimental condition we have assumed x^* as the radius of the laser beam and $D = 120\ \text{cm}^2/\text{s}$.[10]

$J_i(0)$ is the ion current density at the cathode surface:

$$J_i(0) = eN_i(0)v_i(0), \tag{6}$$

where $N_i(0)$ is the atomic ion density with velocity $v_i(0)$. The model of the electric field in the cathodic region developed in Ref. 7 allows us to derive $J_i(0)$ as a function of the Ne mass m_{Ne}, the mean free path l for charge transfer at the pressure p, the Crookes dark-space extension d, and the cathode voltage fall V_c. The result in MKS units is

$$J_i(0) = e(2V_c\epsilon_0/ed^2)\{2(eV_c/m_{\text{Ne}}) \times [2l/d - (1/d)^2]\}^{1/2}. \tag{7}$$

Finally, $J_d(0)$ and $J_g(0)$ are the fluxes of the VUV photons that are created by the electron excitation of the radiative levels in the dark space and in the negative glow region, respectively, and which arrive at the cathode. As a function of the electron current density J^-, these are given by

$$J_d(0) = \eta_d f_d n_d J^-(0), \tag{8}$$

$$J_g(0)\eta_g f_g n_g J^-(d), \tag{9}$$

where n_d and n_g are the numbers of VUV photons created by each electron entering the Crookes space and the negative glow, respectively; and f_d and f_g are their geometric factors for their collection at the cathode. The n_d and n_g numbers may be expressed as a function of the discharge parameters on the basis of the models discussed in Refs. 7 and 8:

$$n_d = [\exp(\alpha pd) - 1], \tag{10a}$$

$$n_g = V_c/[2E_{\text{in}}(\alpha pd)^2], \tag{10b}$$

E_{in} being the mean energy loss for the neon ionization or excitation by the electrons, i.e., 18 eV. Typical values in our pressure and current experimental range for n_d are between 1 and 3 and for n_g between 1 and 10.

In our experimental arrangement the geometric values f_d and f_g are both approximated by

$$f_{d,g} = (1/\pi)\tan^{-1}[b/(2d)],$$

where b is the cathode width. The J_d and J_g fluxes also contain reduction factors η_d and η_g taking into account the VUV photon absorption along the path to the cathode surface. The lifetimes of the involved VUV transitions have been corrected by radiation trapping following the calcula-

tions reported in Ref. 6. The decay rates for the $1s_2$ and $1s_4$ levels were found to be 1.7×10^6 and $3.2\times10^5\ s^{-1}$, respectively, at 1-Torr neon pressure.

By combining Eqs. (2)–(9) and making the reasonable assumption $J^-(d)=J$, we obtain a relation $I(V_c)$ connecting the discharge current I to the cathode fall voltage V_c. In our experimental configuration where the remaining discharge has a small voltage drop, V_c is nearly equal to the external applied voltage. The final current-voltage relation is:

$$I(V_c)=\left(V_c^{3/2}k\frac{1-D+\gamma_i}{1-D-G}+\frac{M}{1-D-G}\right)S, \quad (11)$$

where

$$k=\frac{2\epsilon_0}{d^2}\left\{\frac{8}{em_{\mathrm{Ne}}}\left[\frac{2l}{d}-\left(\frac{l}{d}\right)^2\right]\right\}^{1/2},$$

$$D=f_d n_d \eta_d \gamma_p,$$

$$G=f_g n_g \eta_g \gamma_p,$$

$$M=eD_m\alpha\gamma_m \exp(-\alpha x^*)\mathscr{M}(x^*),$$

and S is the cathode surface area. Equation (11) describes the unperturbed discharge and represents an important step towards an optogalvanic model.

When laser radiation excites a $1s\rightarrow2p$ neon transition, the metastable $1s_{5,3}$ and radiative $1s_{4,2}$ level populations are modified. Consequently, the variations of the metastable density $\Delta\mathscr{M}$ and of the VUV photon densities Δn_d and Δn_g induce a perturbation ΔI of the discharge current. In the regime of low laser intensities and small modifications of the discharge properties, a perturbative development of the current relationship gives

$$\Delta I=\frac{\partial I}{\partial n_d}\Delta n_d+\frac{\partial I}{\partial n_g}\Delta n_g+\frac{\partial I}{\partial \mathscr{M}}\Delta\mathscr{M}. \quad (12)$$

A convenient expression for analyzing the perturbation ΔI of the discharge current, i.e., the OG signal, is obtained by introducing the following quantities:

$$\Delta G=\eta_g f_g \gamma_p \Delta n_g, \quad \Delta D=\eta_d f_d \gamma_p \Delta n_d,$$

$$\Delta M=eD_m\alpha\gamma_m \exp(-\alpha x^*)\Delta\mathscr{M},$$

so that

$$\Delta I=\{J_i(0)[(G+\gamma_i)\Delta D+(1-D+\gamma_i)\Delta G] + M(\Delta G+\Delta D) + (1-D-G)\Delta M\}[S/(1-D-G)^2]. \quad (13)$$

The quantities Δn_d and Δn_g may be expressed as a function of the laser modification for the radiative level populations in the negative glow and dark space:

$$\frac{\Delta n_g}{n_g}=\left.\frac{\Delta\mathscr{R}}{\mathscr{R}}\right|_{\mathrm{glow}}, \quad (14a)$$

$$\frac{\Delta n_d}{n_d}=\left.\frac{\Delta\mathscr{R}}{\mathscr{R}}\right|_{\mathrm{dark}}. \quad (14b)$$

Equation (13) represents an analytical description of the optogalvanic signal in the cathodic region taking into account the contribution of all the secondary electron emission processes.

III. EXPERIMENT

A. Apparatus

Our experimental setup allowed simultaneous optogalvanic and fluorescence spatial observations (Fig. 2). A broadband dye laser (Coherent, model 599-03), tunable in the range of rhodamine 6G, was mechanically chopped at 500 Hz. The laser beam, of 0.1-cm radial dimension, reflected on a translatable mirror M1, passed through the discharge tube parallel to the cathode surface. Spatial analysis of the OG signals was possible by translating the M1 mirror.

Two plane-parallel electrodes, 4 cm apart, were contained inside the cylindrical Pyrex cell. The cathode, with surface dimensions 10.6 cm$\times$1.2 cm, was encased in glass. This reduced the edge discharge effects and the laser beam crossed a very uniform electric discharge region.

The discharge current was limited by a 100-kΩ ballast resistor, and the optogalvanic signals were analyzed using a lock-in amplifier. A second translatable mirror M2, together with the optical system L, reproduced the discharge image on the entrance slit of a Jobin-Yvon monochromator, allowing a spatial fluorescence analysis of the discharge, with spatial resolution limited by the 60-μm entrance slit of the monochromator.

Figure 3 reports the spatial behaviors of the 585.2-nm neon line at different pressures and currents. The dark space, characterized by a low level of fluorescence intensity, occupies the first few millimeters of the discharge region. The strong fluorescence signal is due to the negative glow; the decrease in the signal at large cathode distances obeys an exponential law, consistent with the diffusive motion of the electrons in this region.

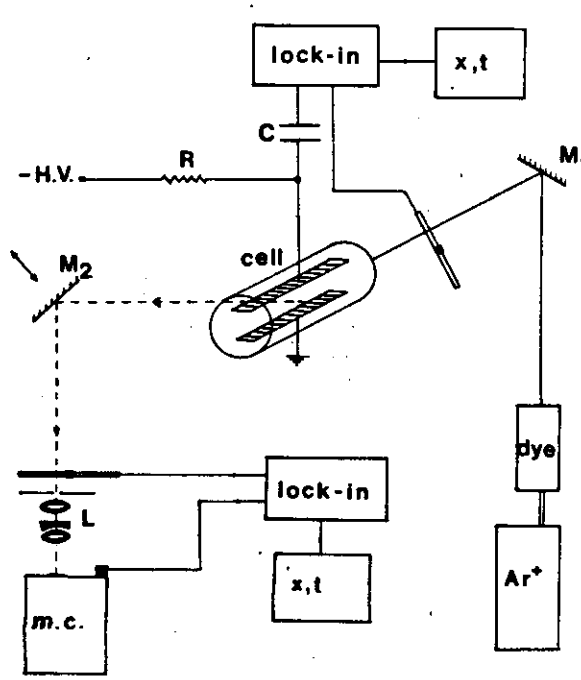

FIG. 2. Experimental setup: M1 and M2, translatable mirrors; m.c., monochromator; L, lens system; R, ballast resistor; C, coupling capacitor; x,t, chart recorder.

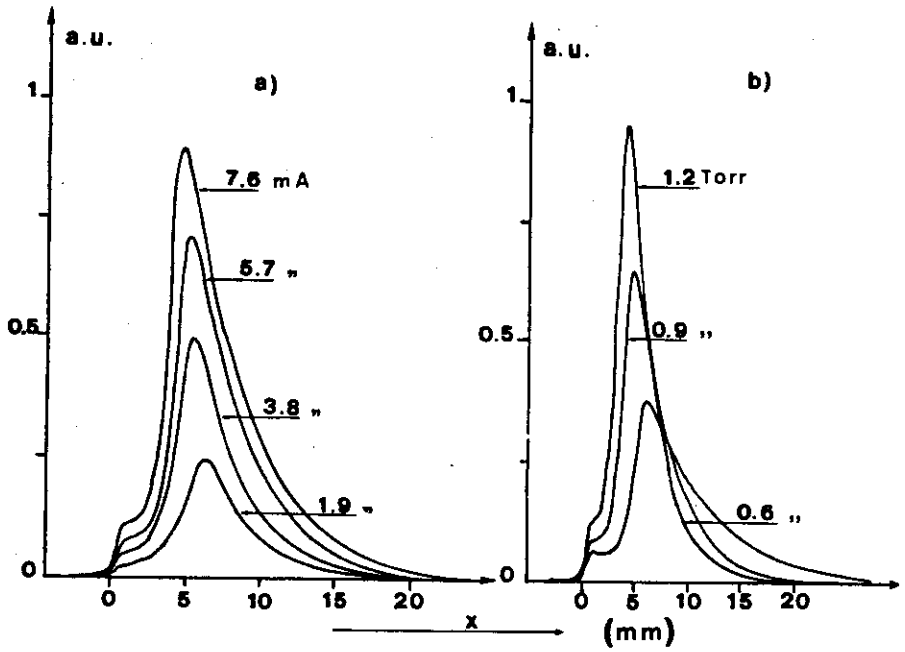

FIG. 3. Experimental spatial behavior of the 585.2-nm fluorescence line at different pressures and currents. In (a) the pressure was fixed to 0.9 Torr, while in (b) the current was fixed to 6.6 mA.

B. Unperturbed discharge

The metastable Ne density in the $1s_5$ level was measured with a standard absorption technique, but due to the low metastable density, a stabilized single-frequency dye laser (Coherent, model 599-21) was used. The absorbed laser intensity was monitored with the discharge switched on and off. At 0.5 Torr, the lowest operating pressure of our discharge where the estimated metastable density is of the order of 10^7 atoms/cm^3, no absorption signal was detected, while the OG signal-to-noise ratio was still very high, approximately 50. At higher pressures typical experimental results for the $1s_5$ level density N_5 in the dark space (d.s.) and in the negative glow (n.g.) are reported in Table I. The measured metastable density values are two or three orders of magnitude lower than those reported in previous experiments in the neon positive column.[6,11] On the basis of the positive column results[6] the N_5 density was assumed equal to 80% of the total metastable density.

Equation (11) has allowed us to make a comparison between the experimental and theoretical current-voltage relationship at different neon pressures, making use of the discharge parameters reported in Table II, which are derived from the literature. The measured metastable atom density in the dark space and the Crookes space extension have been introduced in Eq. (11). The theoretical curve and the experimental points for the (I,V_c) relations are shown in Fig. 4. The good agreement between the laser unperturbed theoretical and experimental I-V_c characteristics is an important step towards the following description of optogalvanic mechanisms in the cathodic region.

C. Perturbed discharge

We have already mentioned that the electrical properties of the cathodic region change as a function of the distance from the cathode surface. So it was not a surprise in the experiment when the magnitude and the sign of the OG signal varied as different parts of the cathodic region were irradiated by neon resonant laser radiation.

Figure 5 reports typical OG spatial behaviors for two laser wavelengths, (a) 588.2 nm and (b) 603.0 nm, involving laser excitation from the metastable $1s_5$ and radiative $1s_4$ levels, respectively, with 100-mW broadband laser power. For the sake of completeness we have also reported in Fig. 5(c) the spatial behavior of the 585.2-nm fluorescence line. Relative OG and fluorescence measurements at different current and pressure values are reported.

The OG signals for laser irradiation very close to the cathode are modified by the finite transverse dimension of the laser beam. The increase in the OG signal as a function of the cathode distance originates because at grazing irradiation the cathode intersects the laser beam. As shown in Fig. 5

TABLE I. Metastable density measurements in the dark space (d.s.) and negative glow (n.g.).

N_5 (10^9 atoms/cm^3)		p(Torr)	I (mA)
1.1	d.s.	1.4	4.4
4.6	n.g.		
0.8	d.s.	1.1	2.2
0.3	n.g.		

TABLE II. Discharge parameters of the cathodic region obtained from the quoted references.

		Reference(s)
γ_i	0.06	8, 12
γ_m	0.3	13
γ_p	0.1	7, 8
α	2 (cm Torr)$^{-1}$	8, 15
l/p	0.018 cm/p (Torr)	14

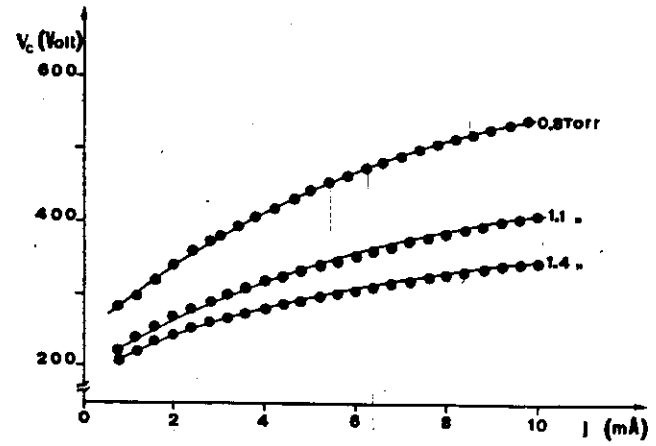

FIG. 4. Comparison between experimental and theoretical behavior of I-V characteristic of three different pressures: 0.8, 1.1, and 1.4 Torr. The dots represent measurements whose accuracy is masked by the dot dimensions. The continuous lines are theoretical curves.

the behavior of the OG signal versus the distance from the cathode is very different depending upon whether a metastable level or a radiative one is involved. The OG spatial dependence was the same for all the laser-induced excitations from

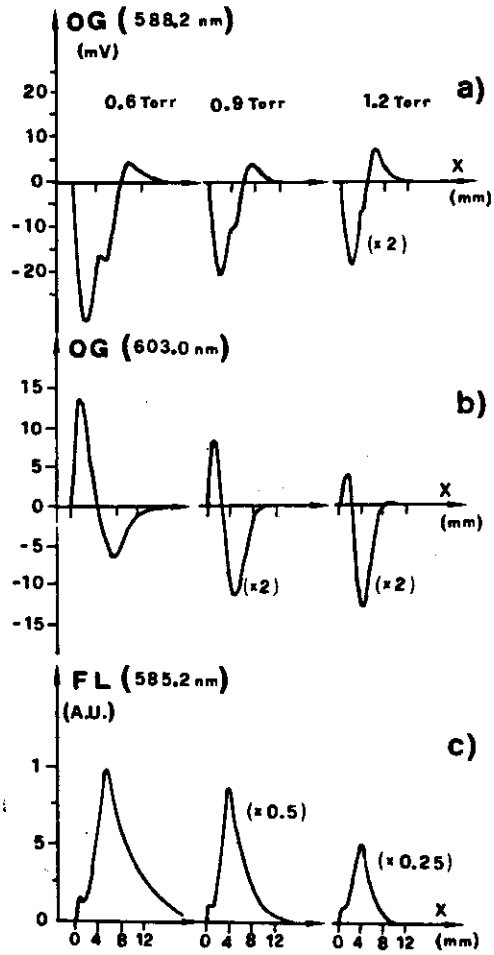

FIG. 5. Experimental OG and fluorescence signals as a function of the distance from the cathode surface: (a) OG for laser-induced excitation at 588.2 nm ($1s_5 \rightarrow 2p_2$); (b) OG for laser-induced excitation at 603.0 nm ($1s_4 - 2p_2$); (c) laser-unperturbed fluorescence from $2p_1$ to $1s_2$. The discharge current was 4 mA while 0.6, 0.9, and 1.2 Torr pressures, respectively, were used.

the metastable levels, as well as from the radiative levels. For radiative level transitions a change of the OG sign occurs when irradiation is moved from the Crookes space to the negative glow.

The OG mechanism based on the perturbation of electron-impact ionization for the laser-excited species has been successfully used in interpreting the OG positive column region.[5] The results of Fig. 5 show that this mechanism is not responsible for the OG effect in the cathodic region. If it was, the spatial dependence of the OG signal would follow the metastable density distribution existing in the Crookes space and in the negative glow. The metastable density distribution is probed by the fluorescence signal, and the comparison of the negative glow OG signal with the fluorescence shows that the modification of the OG signal does not follow that of the metastable population density.

We have also tried to analyze the OG signal by introducing a higher electron collision rate in the negative glow region, which would lead to an enhancement for the multistep ionization rates of the laser excited $2p$ levels. This mechanism is effective in the OG positive column at large current.[5,6] A large electron ionization rate could explain the sign change in the metastable level OG signals, but it is not able to explain why a large OG signal is obtained in the dark space, where the metastable population is small. Moreover, this mechanism cannot explain the reversed sign in the radiative level OG signal in Fig. 5(b).

The OG analysis in the cathodic region should be based on the secondary electron production due to the ions, metastable, and VUV photons bombarding the cathodic surface, as described by Eq. (13). We will first show how the sign of the OG signal can be obtained from a simple analysis of the different contribution in Eq. (13).

Let us consider laser excitation of a metastable level which will produce a negative variation of the metastable atom density ($\Delta M < 0$). When the laser passes through the dark-space region, the VUV photon flux in the negative glow is unperturbed ($\Delta n_g = 0$). Thus in Eq. (13) the Δn_d and ΔM terms only contribute to the OG signal. The $\Delta \mathcal{M}/\mathcal{M}$ relative metastable population modification may be evaluated from the previous measurements in the positive column,[6,11] and for the laser power of Fig. 5, $\Delta \mathcal{M}/\mathcal{M} = \Delta M/M = -0.02$ to -0.04. From a numerical evaluation the Δn_d term in Eq. (13) is smaller than the ΔM term by at least an order of magnitude. Thus Eq. (13) leads to a negative OG signal in the dark space (low x values in Fig. 5) as observed in the experiment. The decrease in metastable density produces a negative OG signal through a decrease in the secondary electron emission from the cathode surface collisions. In fact, in Ref. 16 this is the main process invoked in interpreting the OG signal in an obstructed glow discharge. On the other hand, when the laser beam crosses the negative glow region, the VUV photon flux in the dark space is not modified ($\Delta n_d = 0$) while the VUV photon flux in the negative glow is enhanced ($\Delta n_g > 0$) because of the radiative decay from the $2p$ levels to the $1s_{4,2}$ levels followed by VUV emission. If we supposed that the increase of metastable atoms ($\Delta M > 0$) within the negative glow has a negligible role on the current change ΔI, only the term $\Delta n_g > 0$ in Eq. (13) can

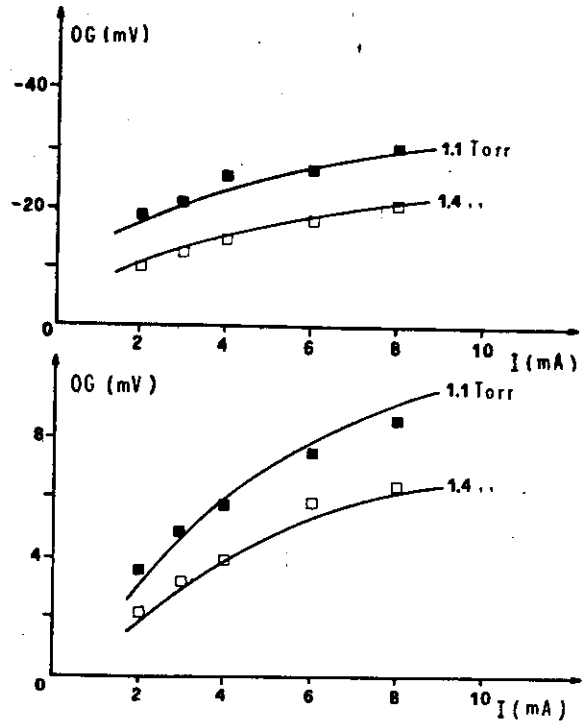

FIG. 6. OG signals vs the discharge current for 588.2 nm irradiation at two different neon pressure values, 1.1 and 1.4 Torr, respectively. (a) Laser beam tangent to the cathode surface; (b) laser beam in the region that produces the maximum OG signal. Continuous lines represent the theoretical results obtained by Eq. (13).

explain the positive variation of the discharge current. Similar considerations can be used to explain the OG sign obtained through the excitation of a radiative level. As a result it appears that Eq. (13) may be used to interpret the OG in the cathodic region and a quantitative analysis may be performed.

The quantitative analysis of the OG signal in the cathodic region making use of Eq. (13) has been based on the following hypothesis or data:

(1) We have derived n_d, n_g, Δn_d, and Δn_g on the basis of Eqs. (10) and (14a) and (14b), making use of the $\Delta\mathcal{R}/\mathcal{R}$ obtained in the following. The final result is that in the dark space the emission of VUV photons is a negligible process and a good approximation is to introduce $\Delta n_d = 0$ in Eq. (13).

(2) The metastable population has been obtained from the absorption measurements with a single-frequency dye laser reported in Sec. III B.

(3) The modification of the metastable density within the negative glow does not affect the discharge current I that, following Eq. (3), depends on the metastable density at the cathode surface.

We have analyzed in more detail through Eq. (13) the OG signal obtained when the laser beam crossed the discharge either tangentially to the cathode surface or within the negative glow region at the x distance with the maximum OG production. There the OG interpretation is more straightforward because in these two particular discharge regions the OG signals are produced respectively by the metastable variation ($\Delta\mathcal{M}$) at the cathode and by the VUV photon variation (Δn_g). At any other distance from the cathode surface the simultaneous presence of both mechanisms contributes to the OG signal, and, for instance, produces the zero crossing of the OG signal.

Figure 6 shows the OG signal induced by 588.2-nm ($1s_5 \rightarrow 2p_2$) irradiation as a function of the discharge current at two neon pressure values. Figure 6(a) is for laser irradiation tangent to the cathode, while Fig. 6(b) was obtained for irradiation of the negative glow region corresponding to the maximum OG production. The continuous curves represent the theoretical result obtained from Eq. (13) under the assumptions described above in points (1) and (2). The continuous lines of Fig. 6 were obtained by a proper choice of the relative variation in the metastable population at the cathode and in the radiative level population within the negative glow. Thus the following values are obtained for the best agreement between Eq. (13) and experimental results:

at 1.1 Torr,

$$\Delta M(0)/M(0) = -0.032(2), \quad \Delta\mathcal{R}/\mathcal{R} = 0.020(2);$$

at 1.4 Torr,

$$\Delta M(0)/M(0) = -0.020(2), \quad \Delta\mathcal{R}/\mathcal{R} = 0.010(2).$$

These relative variations are in agreement with the measurement in the positive column made in Refs. 6 and 11.

IV. CONCLUSIONS

We have demonstrated that the impedance changes observed in the cathodic region of a glow discharge upon resonant laser irradiation are due to different mechanisms. From an analysis of the OG signals observed for laser irradiation at different positions within the cathodic region, it is shown that different mechanisms are strictly related to the OG spatial dependence. A dominant role in sustaining the glow discharge and producing the OG signal is played by the bombardment of the cathode surface by metastables, VUV photons, and ions. The depletion of the metastable atoms by laser excitation to a level cascading to the neon ground state is the source of the negative OG signals, as pointed out also for the neon obstructed glow.[16] The increase of UV photons by neon atoms in the so-called radiative levels is the source of the positive OG signals.

The observations of the fluorescent emission and of the laser absorption have been used to determine the relevant parameters of our glow discharge. The observation and fit of the (V,I) characteristics have been used to check the proper correspondence of the theoretical model to our system. We made use of this understanding of the discharge to interpret our OG results. The values for the modification of the relative population under laser irradiation of both metastable and radiative levels result in agreement with the positive column measurements to within a few percent.

The OG modeling presented in this paper may be relevant also to other discharges where laser perturbation of the cathode bombardment is the dominant process. For instance, a proper treatment of this bombardment should be included in a quantitative analysis of hollow cathode discharges.

ACKNOWLEDGMENTS

The authors thank Professor M. Inguscio for the precious loan of instrumental parts used in this experiment and Professor R. Bernheim for a careful reading of the manuscript.

[1]See, for example, the papers published in the issue J. Phys. (Paris) C7 (1983).
[2]C. Dreze, Y. Demers, and J. M. Gagné, J. Opt. Soc. Am. 72, 912 (1982).
[3]E. F. Zalenski, R. A. Keller, and R. Engleman, J. Chem. Phys. 70, 1015 (1979).
[4]R. Shuker, A. Ben-Amar, and G. Erez, Opt. Commun. 42, 29 (1982).
[5]K. C. Smyth and P.K. Schenck, Chem. Phys. Lett. 55, 466 (1978).
[6]D. K. Doughty and J. E. Lawler, Phys. Rev. A 28, 773 (1983).
[7]P. F. Little and A. Von Engel, Proc. R. Soc., London Ser. A 224, 209 (1954).
[8]A. Von Engel, *Ionized Gases* (Clarendon, Oxford, 1965).
[9]R. W. Engstrom and W. S. Huxford, Phys. Rev. 58, 67 (1940).
[10]L. B. Loeb, *Basic Processes of Gaseous Electronics*, (University of California Press, San Francisco, 1961), p. 880.
[11]M. G. Di Vito, A. Sasso, and E. Arimondo (unpublished).
[12]M. J. Druyvesteyn and F. M. Penning, Rev. Mod. Phys. 12, 87 (1940).
[13]H. S. Massey and E. H. S. Burhop, *Electrons and Ions Impact Phenomena* (Clarendon, Oxford, 1952).
[14]W. D. Davis and T. A. Vanderslice, Phys. Rev. 131, 211 (1963).
[15]S. C. Brown, *Basic Data of Plasma Physics* (Chapman and Hall, London, 1959).
[16]D. K. Doughty and J. E. Lawler, Appl. Phys. Lett. 42, 34 (1983).

Reprinted from Journal of the Optical Society of America B, Vol. 5, page 1484, July 1988

Simultaneous optogalvanic and laser-induced fluorescence investigation in the neon positive column

A. Sasso and M. Ciocca

Dipartimento di Fisica Nucleare, Struttura della Materia e Fisica Applicata, Università di Napoli, Pad. 20 Mostra d'Oltremare, 80125 Napoli, Italy

E. Arimondo

Dipartimento di Fisica, Università di Pisa, Piazza Torricelli 2, 56100 Pisa, Italy

Received May 19, 1987; accepted February 25, 1988

The optogalvanic effect in the positive column of a neon discharge has been investigated both experimentally and theoretically. A mechanically chopped dye laser was tuned to several $1s_i$–$2p_j$ neon transitions (Paschen notation). Optogalvanic spectra and their dependence on the current (1–5 mA) for the 594.5-nm optogalvanic resonance were analyzed. Furthermore, fluorescence and laser-induced fluorescence from the discharge have been examined. A general model based on the steady-state solution of rate equations has been developed in order to interpret the optogalvanic and fluorescence measurements. Good agreement between optogalvanic measurements and theoretical predictions was obtained, but there is a discrepancy between the theoretical prediction and the observed laser-induced fluorescence, which exposes the limitations of the model.

INTRODUCTION

Optogalvanic (OG) detection of atoms or molecules may be accomplished by perturbing the electrical equilibrium of a gas discharge through laser radiation that is resonant with a transition of a species contributing to the discharge mechanisms. OG detection is based on a change in the discharge impedance or, equivalently, a variation in the discharge current. Because of its simplicity, high sensitivity, and selectivity, this technique has been successfully used in a wide variety of laser-spectroscopy experiments, as shown in Refs. 1 and 2.

The OG phenomenon represents a sensitive probe of the population distribution in an atomic or molecular system. The fluorescence spectrum represents an alternative well-established technique for obtaining information on this population distribution. If OG and fluorescence spectra are simultaneously recorded, however, it turns out that for different transitions the OG and fluorescence signals exhibit different behaviors. Thus separate excitation/deexcitation mechanisms are monitored by the two techniques. As an example of this we show in Fig. 1 both OG and fluorescence spectra recorded in our experiment in a neon positive column. Figure 1 also shows the result of an optoacoustic (OA) investigation[3] to make clear that each technique probes a separate mechanism. Thus, by using the technique in Ref. 3, a gas discharge may be thoroughly studied. The present work is concerned with OG and fluorescence mechanisms.

To understand the mechanisms leading to the OG signal, several experiments were carried out in different kinds of discharges and flames. Steady-state[4–8] and transient OG[9,10] regimes were investigated by means of cw and pulsed laser sources, respectively.

Quantitative models able to interpret OG signals were obtained under limited experimental conditions. The difficulty in developing a more general model is due to the large number of parameters that characterize a discharge system. Moreover, knowledge of the operating characteristics of a particular discharge is largely empirical. Nevertheless, a well-developed description of the positive column in a normal discharge[11] has permitted us to interpret precisely the OG mechanisms in the positive column.[12]

Together with single-step electronic collisions, two-step and multistep collisions are the dominant ionization processes of neon atoms in the positive column. In two-step ionization processes the $1s_i$ levels are populated by the process

$$\mathrm{Ne}(^1S_0) + \mathrm{e}^- \rightarrow \mathrm{Ne}(1s_i) + \mathrm{e}^-, \tag{1}$$

and they are ionized through the collisions

$$\mathrm{Ne}(1s_i) + \mathrm{e}^- \rightarrow \mathrm{Ne}^+ + 2\mathrm{e}^-, \qquad i = 2, 3, 4, 5. \tag{2}$$

In the multistep ionization process the $1s_i$ ionization occurs through the highly excited $2p_j$ levels:

$$\mathrm{Ne}(1s_i) + \mathrm{e}^- \rightarrow \mathrm{Ne}(2p_j) + \mathrm{e}^-, \tag{3}$$

$$\mathrm{Ne}(2p_j) + \mathrm{e}^- \rightarrow \mathrm{Ne}^+ + 2\mathrm{e}^-. \tag{4}$$

The neon levels have been indicated in Paschen notation. For both two-step and multistep ionization processes, the role played by metastable $1s_i$ neon atoms is essential.

Irradiation of a positive column discharge by laser light that is resonant with the $1s_{5,3} \rightarrow 2p_j$ transition results in depletion of the population of metastable $1s_{5,3}$ levels and reduces the rates of Reactions (2) and (3). Consequently the electron density decreases, and a negative OG signal results. When the laser excites a transition from a radiative $1s_{4,2}$ level, however, the metastable density is increased by the spontaneous decay from the upper $2p_j$ laser-excited level down to the $1s_{5,3}$ levels. In this case both the ionization processes and the discharge current are increased, so that a

0740-3224/88/071484-08$02.00

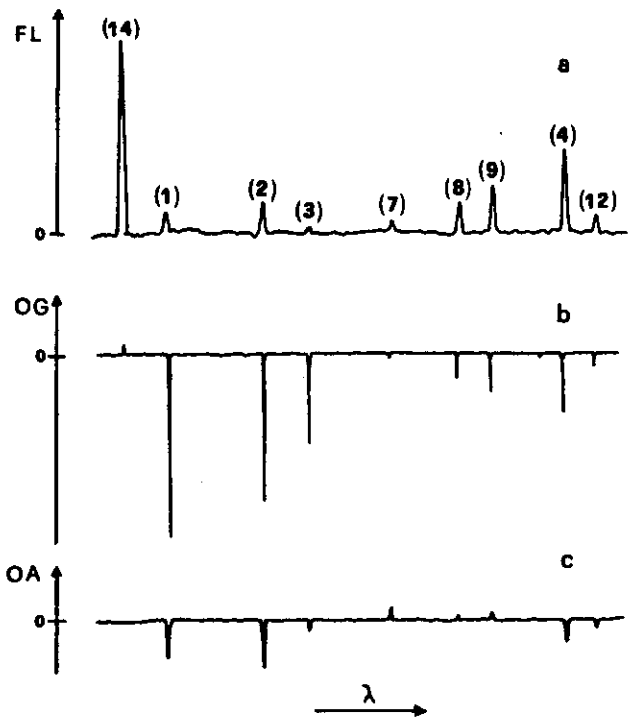

Fig. 1. Neon transitions between 580 and 620 nm observed with three different techniques: (a) the fluorescence spectrum, (b) the OG spectra and (c) the OA spectra. The spectra were recorded at 2.7-Torr neon pressure and 3-mA discharge current. The neon transitions with their assignments are listed in Table 2.

positive OG signal is obtained. This description does not take into account other competitive effects that contribute to the OG phenomenon. For example, at high current and/or at high laser intensity, where a large $2p_j$ population is produced, the ionization Reaction (4) from the laser-excited upper level can be more efficient than Reaction (2) from the laser-depleted level. This mechanism produces a positive OG signal that has been detected.[13]

A description of the main features in the neon positive-column OG effect at low current and weak laser power has been derived in Refs. 12 and 14. Those models are, however, oversimplified because (i) they do not separate the contributions of the $1s_5$ and $1s_3$ metastable levels and of the quasi-metastable $1s_4$ radiative levels, and (ii) they do not include collisional mixing between the upper $2p_j$ level with neighboring levels. Thus, although the model of Ref. 12 has been successfully applied to describe the OG effect on the 594.5-nm $1s_5$–$2p_4$ line, it cannot be applied to an overall OG spectrum and the fluorescent emission as well.

In this paper we present a thorough study of the neon positive column under resonant laser irradiation. The OG signals for different laser-excited transitions have been measured as functions of pressure and current of the neon positive-column discharge. Furthermore, the neon fluorescence spectra from the discharge and the laser-induced fluorescence (LIF) spectra have been recorded in order to probe independently the discharge operation. These measurements have been analyzed through a detailed discharge model that considers separately the contribution of each of the $1s_i$ levels and includes collisional mixing for both the $1s_i$ and the $2p_j$ levels. Our approach leads to a general, but detailed, OG model of the neon positive column. This model may be used to analyze the OG signals observed on a large set of neon transitions. Furthermore, it may also be used to derive the $2p_j$ populations that are essential for the analysis of the fluorescence spectra. Still, our description cannot completely model the emission spectrum.

THEORY

This section presents the detailed steady-state rate equations that describe the populations of the $1s_i$ and $2p_j$ neon levels. The scheme of the relevant neon levels contributing to the OG signal production and their principal excitation and deexcitation mechanisms are shown in Fig. 2.

As mentioned above, the metastable and radiative $1s_i$-level populations are produced by the excitation process of Reaction (1). The rate constants $G_i^{(s)}$ have a strong dependence on E/p, where E is the axial electric field in the positive column and p is the neon pressure. The excitation coefficients for the production of neon atoms in $1s_i$ levels through collisions with low-energy electrons have been measured in Refs. 15 and 16. Their values are reported in Table 1. Radiative decay from the high $2p_j$ levels also contribute to the populations of the $1s_i$ levels. The spontaneous emission coefficients of the $2p_j$–$1s_i$ neon transitions have been

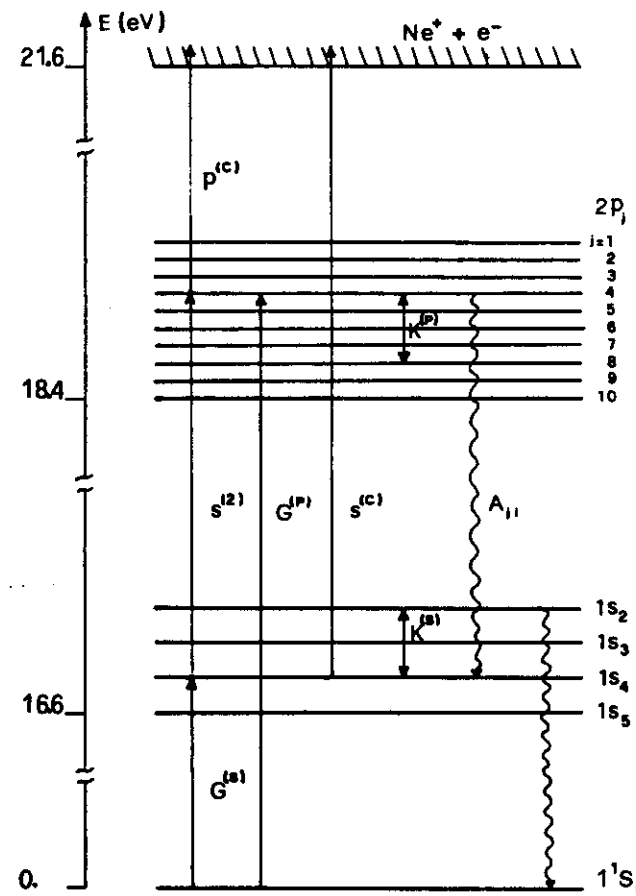

Fig. 2. Simplified energy-level diagram for neon including the $^1S_0$ ground state, the four levels $1s_i$ ($i = 2, 3, 4, 5$), the ten $2p_j$ levels ($j = 1, 2, \ldots, 10$), and the continuum. The main processes of electron-impact excitation, radiative decay, and collisional mixing are schematically represented.

Table 1. Values for the Principal Rate Coefficients of Our Discharge Referred to 0.8-Torr Pressure and 1-mA Discharge Current

Rate Coefficients	Value	Ref.
$G_5^{(s)}$	0.27×10^{-10} cm^3 sec^{-1}	15
$G_4^{(s)}$	0.23×10^{-10} cm^3 sec^{-1}	15
$G_3^{(s)}$	0.32×10^{-10} cm^3 sec^{-1}	15, 16
$s_5^{(c)}$	10^{-8} cm^3 sec^{-1}	17
$p^{(c)}$	2×10 cm^3 sec^{-1}	14
T	2.6×10 cm^3 sec^{-1}	18
D_0	173 cm^2 sec^{-1} Torr	19
KT_e	4.8 eV	20
$D_a(2.4/r)^2$	2.2×10^6 sec^{-1}	12, 21

reported in Ref. 22. At the pressures of our experiment, radiation trapping modifies the $2p_j$-level lifetime, and in the numerical analysis a trapped lifetime $(A_{ji})^{-1}$, modified in accordance with the Holstein formula[23] for trapping by the transverse dimension of the cylindrical discharge, has been used. Population transfer between the $1s_i$ levels produced by collisions with ground-state neon atoms (N_g) is represented by the rate constant $K_{ij}^{(s)}$ taken from Ref. 24 for the transfer from the i to the j level.

The loss channels for the $1s_i$ levels are the following ones:

1. Collisions with electrons producing direct ionization [process (2)] with rate constants $s_i^{(c)}$ (Ref. 25);
2. Collisions with electrons producing Ne($2p_j$)-excited neon atoms [process (3)] with a rate constant taken to be independent of the specific level, $s_i^{(p)} = s^{(p)}$ (Ref. 17);
3. Collisions between two excited Ne($1s_i$) atoms, producing associative ionization. The rate T of this process was assumed equal to the rate of the equivalent process in helium reported in Ref. 18.

Other specific processes contribute to the deexcitation of the metastable or radiative $1s_i$ levels. Metastable losses may result from diffusion and deexcitation on the cell wall and from two-body collisions. If D_0 is the diffusion coefficient for the metastable neon atoms at 1 Torr, the metastable loss rate is[19]

$$w_i = (D_0/p)\Lambda^{-2} + Ap \qquad \text{for } i = 5, 3, \tag{5}$$

where $\Lambda = (r/2.405)$ is the diffusion length, r is the radius of the positive column, A is the frequency of destruction by two-body collisions at 1 Torr, and p is the neon pressure measured in Torr. The $1s_4$ and $1s_2$ levels are radiatively coupled to the $^1S_0$ ground state with lifetimes 1.6×10^{-8} sec and 1.2×10^{-9} sec (Ref. 24) and transitions at wavelengths $\lambda_4 = 74.37$ nm and $\lambda_2 = 73.59$ nm, respectively. The lifetime of the $1s_2$ level is strongly increased by radiation trapping and, being that the transition $1S_0$–$1s_2$ is pressure broadened, the resulting corrected lifetime is independent of pressure[23] and results in

$$w_2 = [\tau_2]_{\text{trap}}^{-1} = 1.65 \times 10^6 \text{ sec}^{-1}. \tag{6}$$

In our experimental pressure range the $1S_0$–$1s_4$ transition is Doppler broadened around 1 Torr and becomes pressure broadened at 10 Torr. Doughty and Lawler[12] calculated the following $1s_4$ decay rate by extrapolating between these two regions:

$$w_4 = [\tau_4]_{\text{trap}}^{-1} = \begin{cases} 3.2 \times 10^5 \text{ sec}^{-1} & p = 1 \text{ Torr} \\ 1.4 \times 10^5 \text{ sec}^{-1} & p = 5 \text{ Torr} \end{cases}. \tag{7}$$

If all the processes listed above are included, the rate equations for the $1s_i$-level S_i populations are

$$\frac{d}{dt} S_i = +G^{(s)} N_g n_e + \sum_{j=1}^{10} A_{ji} P_j + N_g \sum_{\substack{j=2 \\ j \neq i}}^{5} K_{ji}^{(s)} S_j - N_g S_i \sum_{\substack{j=2 \\ j \neq i}}^{5} K_{ij}^{(s)} - [s^{(p)} + s_i^{(c)}] S_i n_e - TS_i \sum_{j=2}^{5} S_j - w_i S_i - \sigma F_L \left(S_m - \frac{g_m}{g_n} P_n \right) \delta(i = m), \qquad i = 2, 3, 4, 5, \tag{8}$$

where P_j describes the $2p_j$-level population. In these equations we have included the laser-absorption and stimulated-emission processes of the S_m and P_n populations of the $1s_m$ and $2p_n$ levels perturbed by the radiation. σ is the absorption cross section of the laser-excited transition, F_L is the photon flux of the laser beam, and g_m and g_n are the statistical weights of the laser-excited $1s_m$ and $2p_n$ levels, respectively.

The populations of the $2p_j$ levels are produced by electron-impact excitation from the ground state with rates $G_j^{(p)} = G^{(p)}$, by electron-impact excitation from the $1s_i$ levels with the $s^{(c)}$ rates introduced before, or by dissociative recombination of Ne_2^+ ions with density equal to the n_e electron density, as described through the process

$$Ne_2^+ + e^- \rightarrow Ne(2p_j) + Ne(1S_0). \tag{9}$$

The dependence of the dissociative recombination coefficient α_r on the electronic temperature T_e is[17]

$$\alpha_r = \frac{2.5 \times 10^{-4}}{(T_e)^{1/2}} [1 - \exp(-900/T_g)], \tag{10}$$

where T_g is the gas temperature. As shown in Ref. 20, the electronic temperature T_e (in electron volts) is dependent on the $r \times p$ product. The dissociative recombination process uniformly populates the ten $2p_j$ levels, so that the production rate for each level is $\alpha_r n_e^2/10$.

The loss rates for the $2p_j$ levels include electron-impact ionization, i.e., process (4), with rate constant $P^{(c)}$, and the coupling between the $2p_j$ levels through collisions with ground-state neon atoms, with $K_{ij}^{(p)}$ rate coefficients.[26] The rate equations that describe the evolution of the $2p_j$ populations are

$$\frac{d}{dt} P_j = +n_e \sum_{i=2}^{5} s^{(p)} S_i + \frac{\alpha_r}{10} n_e^2 + G^{(p)} N_g n_e + N_g \sum_{\substack{l=1 \\ l \neq j}}^{10} K_{lj}^{(p)} P_l + \sigma F_L \left(S_m - \frac{g_m}{g_n} P_n \right) \delta(j = m) - N_g P_j \times \sum_{\substack{l=1 \\ l \neq j}}^{10} K_{jl}^{(p)} - P_j \sum_{i=2}^{5} A_{ji} - p^{(c)} P_j n_e. \tag{11}$$

Finally, the rate equation for the electron density is

$$\frac{d}{dt}n_e = +n_e\left[\sum_{i=2}^{5} s_i^{(c)}S_i + \sum_{j=1}^{10} p^{(c)}P_j\right] + \alpha_T v_d n_e + \frac{T}{2}\sum_{\substack{j=2\\ j\neq j'}}^{5}\sum_{j'=2}^{5} S_j S_{j'} + T\sum_{i=2}^{5} S_i^{(2)} - D_a\left(\frac{2,4}{r}\right)^2 n_e - \alpha_r n_e^2. \tag{12}$$

The first term on the right-hand side of Eq. (12) represents single-step ionization of ground-state neon atoms. α_T is the first Townsend coefficient, and v_d is the electron-drift velocity. Both of these are functions of the ratio E/p, where E is the axial electric field in the positive column. The ambipolar diffusion loss rate for electrons is given by $D_a\,[(2,4)/r]^2$, where D_a is the ambipolar diffusion coefficient, which, for a neon discharge, was reported in Refs. 12 and 21.

The set of Eqs. (8), (11), and (12), in the steady state, represents a set of 15 nonlinear algebraic equations. We have numerically solved this system for two cases: for laser switched off (unperturbed discharge) and laser switched on (perturbed discharge).

Unperturbed Discharge

We have solved the set of Eqs. (8), (11), and (12) with respect to the populations of the $1s_i$ and the $2p_j$ levels and to the electron density in the absence of laser radiation.

Numerical results for the electron density obtained with discharge parameters summarized in Table 1 are consistent with the direct relationship to the current discharge I,[12] i.e.,

$$I = e\pi r^2 v_d n_e 2h_0, \tag{13}$$

where e is the electron charge and $2h_0$ is a constant defined by Tonks and Langmuir[27] that relates the average and axial electron concentration. For a cylindrical cell, the $2h_0$ constant ranges from 0.42 to 1, according to the ion free path.[28]

The value of the drift velocity v_d in different discharge conditions has been obtained by making use of the well-known relationship $v_d = v_d(E/p)$ reported in Ref. 29. We measured the electric field in the positive column as a function of the discharge current I at different neon pressures, as explained in the experimental section. The first Townsend coefficient α_T has also been obtained from the data reported in Ref. 29 on the basis of the measured E/p values.

The determination of the $2p_j$ and $1s_i$ populations from the numerical solution of Eqs. (8), (11), and (12) permits us to derive the neon fluorescence spectra for different values of the discharge current and neon pressure. A preliminary test was made by introducing into Eqs. (8), (11), and (12) the discharge parameters of the Doughty and Lawler experiment.[12] The computed populations of the $1s_i$ levels and the electron density result in good agreement with the experimental values reported by them.

Table 1 is a list of the principal discharge parameters used in our calculations at 0.8-Torr neon pressure and 1-mA discharge current. The parameters describing the neon discharge were derived from the literature and were included in the rate equations. Thus the comparison between our model and the theoretical analysis represents a test for the description of the model.

Figure 3 shows the $1s_i$ populations versus the discharge current at a fixed neon pressure. The figure also shows the dependence of the electron density as calculated from Eq. (12). Similar behaviors were obtained for the different neon pressures of our experiment. The population distribution over the $1s_i$ levels is well represented by a Boltzmann distribution with an effective 13-eV temperature, determined by the electron collisions.

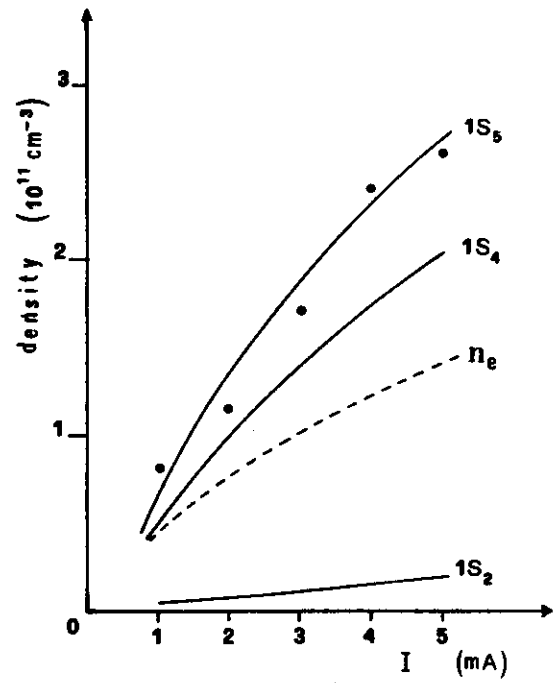

Fig. 3. The $1s_i$ (i = 3, 4, 5) neon level populations as functions of current at 0.8 Torr, as derived from the numerical solution of the rate equations. The dashed line reports the electron density derived from Eq. (14). Points represent the $1s_5$-level density obtained from the absorption measurements.

Perturbed Discharge

When laser radiation is resonant with a $1s_i$–$2p_j$ neon transition, the overall $1s_i$, $2p_j$-levels populations and, consequently, the electron density are modified. The perturbed discharge was analyzed by solving Eqs. (8), (11), and (12) with respect to the electron density n and the populations S_i (i = 2, 3, 4, 5), P_j (j = 1, 10) in the $1s_i$ and $2p_j$ states. This numerical model was applied to determine the laser-perturbed $1s_i$, $2p_j$ populations for a wide range of discharge-current and neon-pressure values.

The OG signal considered as a perturbation in the discharge current is given by the relation

$$\Delta I = e2\pi r^2 h_0\left[v_d(n_e)_{\text{laser on}} + \frac{\partial v_d}{\partial E}\Delta E(n_e)_{\text{laser on}} - v_d(n_e)_{\text{laser off}}\right]. \tag{14}$$

The modification ΔE in the electric field within the discharge is derived by considering that in the experimental arrangement a constant-voltage power supply feeds the discharge tube with length l and a ballast resistor R_b in series with the discharge. Thus

$$l\Delta E + R_b\Delta I = 0 \tag{15}$$

and

$$\Delta I = \frac{e2\pi r^2 h_0 v_d[(n_e)_{\text{laser on}} - (n_e)_{\text{laser off}}]}{1 + e2\pi r^2 h_0 \frac{\partial v_d}{\partial E}\frac{R_b}{l}(n_e)_{\text{laser on}}}. \quad (16)$$

Relation (16) represents the general description of the OG effect in the positive-column region.

Note that our approach is different from that of Doughty and Lawler.[12] Those authors measured the so-called dynamical impedance of the discharge, i.e., the discharge impedance at the modulation frequency, to determine the discharge operation without laser radiation.

EXPERIMENTS

Our experimental setup is shown in Fig. 4. A broadband jet-stream dye laser pumped by an Ar^+ laser was tuned into the range of the Rhodamine 6G dye where most of the $1s_i$–$2p_j$ neon transitions occur. The laser beam was mechanically chopped at 300 Hz.

The discharge tube was a Pyrex cylindrical tube with a 0.25-cm radius and with a length of the positive column of 21.5 cm. The aluminum electrodes were offset from the column axis, so that only the positive column was crossed by the laser beam. The pressure was in the 0.8–5-Torr range, and the current was varied between 1 and 5 mA. The cathode was connected through a ballast resistor (R_b = 100 KΩ) to a voltage-stabilized power supply. The OG signals were detected by means of capacitive coupling and were analyzed with the use of a lock-in amplifier.

The fluorescence from the central part of the positive column was focused on the entrance slit of a 50-cm monochromator. The wavelength-resolved fluorescence spectra were analyzed when the laser beam was switched on or off. In the LIF spectra the difference ΔJ between the fluorescence light with laser on and laser off was recorded using a lock-in detector.

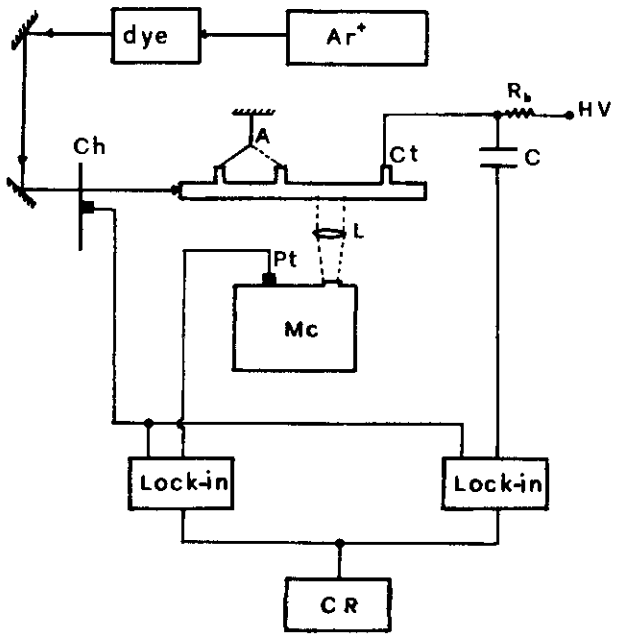

Fig. 4. Experimental setup: Ch, chopper; A, anode; Ct, cathode; Pt, phototube; Mc, monochromator; CR, chart recorder; L, lens; R_b, ballast resistor; HV, high-voltage power supply; C, capacitive coupler.

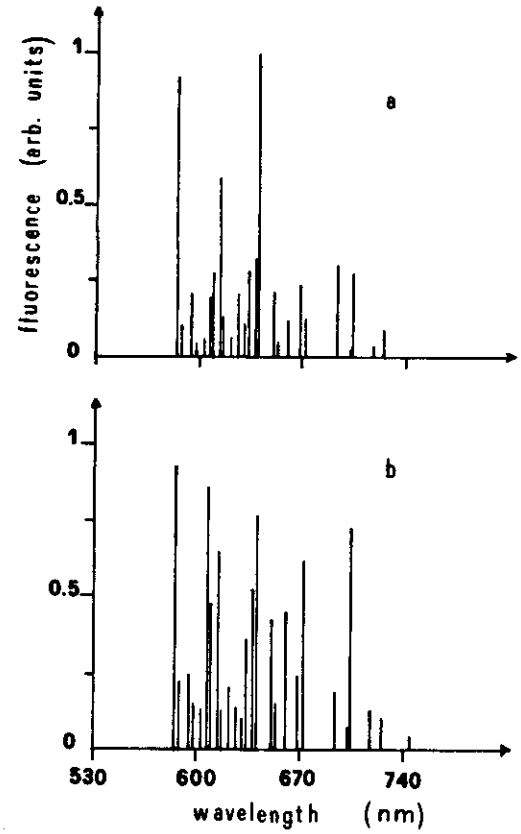

Fig. 5. Comparison between a, experimental and b, theoretical neon fluorescence spectra at 1 mA and 0.8 Torr.

Two anodes at different distances from the cathode allowed us to vary the positive-column length. The discharge voltage measured for the two different positive-column lengths permitted us to derive the positive-column axial electric field, which, to a good approximation, is assumed constant over the positive-column length. The dependence of the electric field on the discharge current I was measured for several values of pressure. As already mentioned, the determination of the dependence of the electric field from the discharge current, with the well-known $v_d(E/p)$ and $\alpha_T(E/p)$ dependences, allows us to obtain the drift velocity and the first Townsend coefficient at the particular pressure and current values of our experiment.

The metastable atom density that appears as a parameter in the equations to be solved numerically was determined with standard absorption techniques. In fact, we have monitored the laser intensity absorbed by the neon positive column in the discharge. With a narrow-band dye laser used in the absorption experiment, a density measurement of good accuracy could be realized. The metastable density was estimated in the 10^{10}–10^{12} atoms/cm^3 range, in good agreement with the results of the rate-equation solution, as shown in Fig. 3. Thus the absorption measurement may be considered as an additional test of the numerical analysis for the population distribution. The metastable density was introduced into the radiation-trapping calculation to correct the spontaneous emission coefficients of the $1s_i$–$2p_j$ transitions for trapping.

Table 2. Wavelengths of the Observed Lines and Their Spectroscopic Assignment (Paschen Notation)

Designation	Neon Transition (Paschen)	Wavelength (nm)
(1)	$1s_5$–$2p_2$	588.2
(2)	$1s_5$–$2p_4$	594.5
(3)	$1s_5$–$2p_5$	597.6
(4)	$1s_5$–$2p_6$	614.3
(5)	$1s_5$–$2p_7$	621.7
(6)	$1s_5$–$2p_8$	633.4
(7)	$1s_4$–$2p_2$	603.0
(8)	$1s_4$–$2p_3$	607.4
(9)	$1s_4$–$2p_4$	609.6
(10)	$1s_4$–$2p_5$	612.8
(11)	$1s_4$–$2p_6$	630.5
(12)	$1s_3$–$2p_2$	616.4
(13)	$1s_3$–$2p_5$	626.6
(14)	$1s_2$–$2p_1$	585.2

Laser-Off Measurements

A typical spectrum of the neon visible fluorescence obtained at 0.8 Torr with $I = 1$ mA is presented in Fig. 5a. The intensity lines were corrected for the phototube and the monochromator grating efficiency. Figure 5b reports the theoretical spectra obtained from the numerical solution of Eqs. (8), (11), and (12) in terms of the unknown variables in Eq. (13). The intensities of the $1s_i$–$2p_j$ transitions were calculated using the standard formula[28]

$$I_{ji}(\omega_{ji}) = \frac{\hbar\omega_{ji}^3}{4\pi^3c^2\left(\frac{g_j}{g_i}\frac{S_i}{P_j} - 1\right)} \times \left\{1 - \exp\left[-\frac{\pi^2c^3r}{\omega_{ji}^3}\frac{A_{ji}}{g_i}\frac{1}{\left(\frac{2\pi KT_g}{M}\right)^{1/2}}(g_jS_i - g_iP_j)\right]\right\}, \quad (17)$$

where $\omega_{ji} = (E_j - E_i)/\hbar$ is the transition frequency between the levels $1s_i$ and $2p_j$, whose energies are E_i and E_j and have statistical weights g_i and g_j, respectively. M is the atomic neon mass, T_g is the translational gas temperature ($\simeq$550 K in our experimental condition), c is the speed of light, and K is the Boltzmann constant.

The experimental and theoretical spectra were normalized independently, assuming that the intensity of the strongest fluorescence line in each spectrum has an intensity equal to 1 in arbitrary units. It appears that the theory does not reproduce exactly the intensities of the fluorescence lines and does present large differences for a few. A discussion of these discrepancies, as well as those detected in other measurements, will be presented below.

Laser-On Measurements

OG Spectra

The tunability range of the Rhodamine 6G dye permits us to excite several $1s_i$–$2p_j$ neon transitions. The transitions ob-

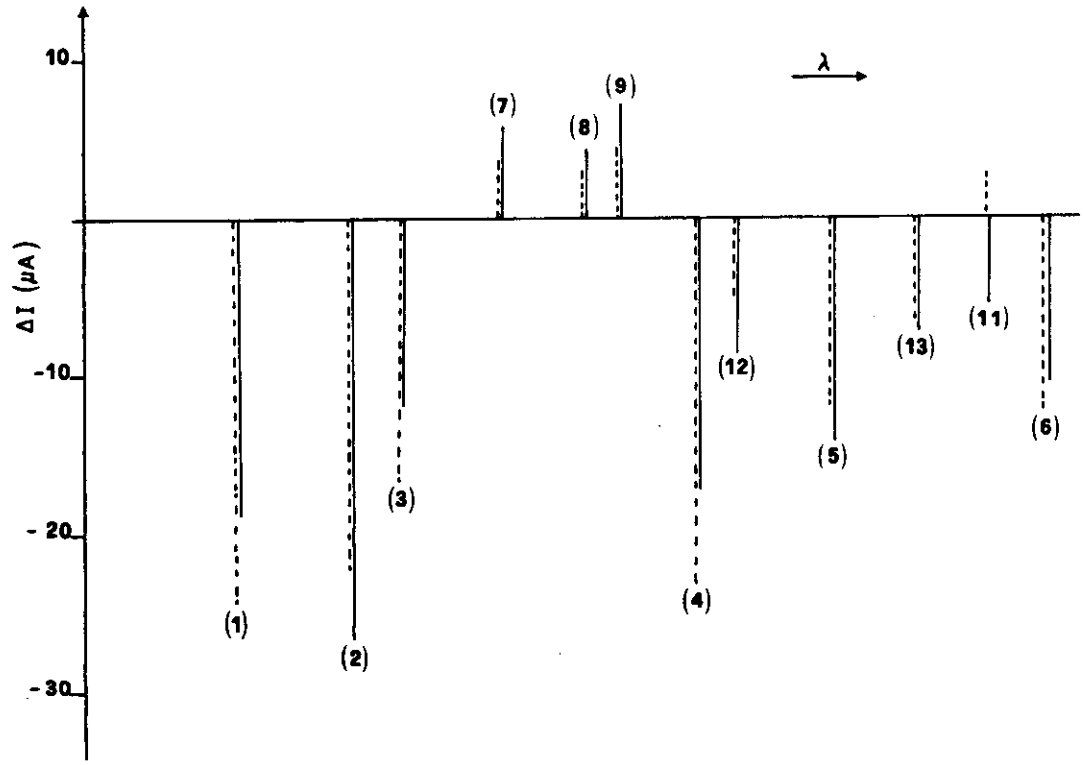

Fig. 6. Experimental (solid lines) and theoretical (dashed lines) OG spectra at 1 mA and 0.8 Torr. The laser-intensity profile in the analyzed spectral range was taken from measured intensity emission of the dye laser. The power at maximum emission (λ = 580 nm) was limited to $\simeq$10 mW to avoid saturation for all the investigated lines. The signal represents the modification (measured in microamperes) of the current flowing through the discharge.

served in the different OG and fluorescence spectra are listed in Table 2. Figure 6 shows an OG spectrum obtained in a low-pressure discharge at low current when the laser was tuned in the range 580–640 nm. In this spectrum the negative OG signals (decrease in current) originate in transitions starting from metastable levels, whereas the positive lines (increase in current) arise from the radiative $1s_4$ level. The dashed lines in the spectrum correspond to the theoretical intensity for the OG lines, as obtained through Eq. (16). The theoretical spectrum was normalized to the experimental one on the basis of the 594.5-nm OG signal discussed below. The agreement for both sign and relative intensity should be considered to be good, owing to the large number of parameters involved in the analysis. In fact, our analysis predicts an OG signal by sign and intensity in agreement with the measured values except for one line (at 630.5-nm wavelength). At this line the sign at the laser power introduced into the theoretical analysis gives results different from the measured one. However, the 630.5-nm line changes sign at a larger laser power ($P_L > 10$ mW), owing to the delicate balance between the different processes contributing to the OG signal. The OG model based on the key role of the metastable atoms, which in Ref. 12 was applied only to the OG signal at 594.5-nm laser excitation, explains the overall neon spectra if properly modified rate equations are solved. Owing to the peculiar behavior of the $1s_4$ level, which under particular experimental conditions behaves as a metastable level because of the radiation trapping, the OG transitions starting from this level can exhibit a negative sign as shown, for example, in the spectra of Fig. 1 taken at a larger pressure than that of Fig. 6.

As a particular case, we analyzed the experimental and theoretical dependence of the 594.5-nm-line OG signal on the discharge current. This line was investigated in Ref. 12 in which a linear, steady-state pertubation theory was used to interpret the experimental results. Figure 7 shows our experimental and theoretical results. The theoretical curve was normalized to the experimental point at 1 mA to take into account the indetermination in the measured laser power. The same normalizing factor was introduced in the theoretical spectrum of Fig. 6. Again, the agreement between theory and experiment is good.

Laser-Induced Fluorescence Spectra

The LIF spectra monitor the modifications in the fluorescence of the $2p_j \rightarrow 1s_i$ transitions under resonant laser excitation. Obviously the increase of the laser-excited $2p_j$-level population enhances the fluorescence lines of the transitions sharing the excited $2p_j$ level. Because of collisional mixing between the $2p_j$ levels, the population of the nearest $2p_j$ levels can also be increased under particular current and pressure conditions. On the other hand, the depletion of the lower $1s_i$ levels reduces the electron-impact excitation of the $2p_j$ levels, as described by Reaction (3). As a result, two competitive mechanisms in the $2p_j$ population are simultaneously present, and the transitions originating from levels that are not strongly coupled by the collisions to the optically excited $2p_j$ level may lead to a decrease in fluorescence intensity.

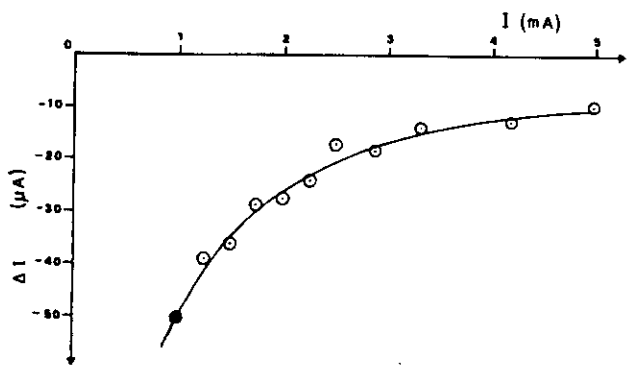

Fig. 7. Comparison between theoretical (solid line) and experimental data (points) for the OG signal on the 594.5-nm laser line versus the current I at 2.7-Torr pressure and 10-mW laser power.

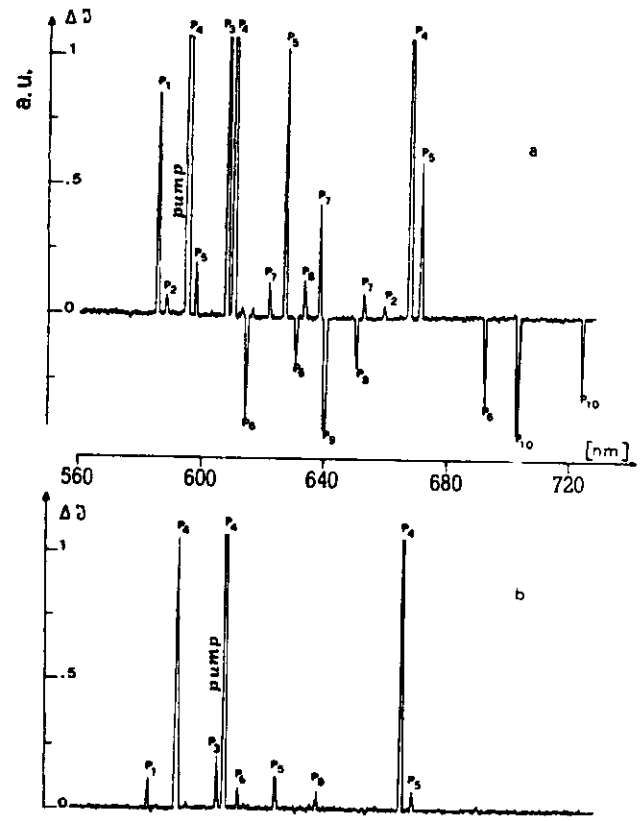

Fig. 8. Experimental laser-induced spectra under laser irradiation of a, the $1s_5$–$2p_4$ transition and b, the $1s_4$–$2p_4$ transition. The values of current and pressure were 3 mA and 1.8 Torr, respectively. For some lines the upper $2p_j$ level of the LIF transition is indicated. Transitions starting from the pumped upper level have a large intensity, which is out of the scale in the record.

Different results are observed for laser transitions starting from metastable or radiative $1s_i$ levels. In fact, when a metastable level is excited by the laser, the impact excitation of $2p_j$ levels is less efficient, and the spectrum exhibits several negative lines, corresponding to a decrease in the fluorescence emission under laser excitation. Figure 8a shows the LIF spectra obtained by exciting the 594.5-nm $1s_5$–$2p_4$ neon transition. The fluorescence lines decreasing in intensity under resonant laser radiation originate from transitions with upper $2p_{6,8,9,10}$ levels. The $2p_7$ level, however, produces a LIF line increasing in intensity, and there is neither a sharp energy separation between levels originating in the positive nor a preference rule for the collisional excitation transfer. Similar results were observed for LIF spectra with excitation from other metastable levels. For instance, we observed

that the $2p_{6,8,9,10}$ levels produce negative LIF lines for irradiation from a metastable to $2p_2$ level, and the $2p_{9,10}$ levels lead to negative lines for laser excitation to the $2p_6$ level.

Completely different LIF spectra were obtained for laser excitation from the radiative $1s_{2,4}$ levels. Figure 8b shows the LIF spectra obtained by excitation of the $1s_4 - 2p_4$ transition at 609.6 nm. Notice that all the transitions from an excited $2p_j$ level are increased in intensity, and no negative lines are observed. Similar observations were made for other LIF transitions involving excitation from radiative levels. These results confirm the key role played by the metastable levels in the excitation of the $2p_j$ levels and, consequently, in the overall balance of the neon discharge.

Our theoretical analysis of the LIF, which is based on the solution of the system of Eqs. (8), (11), and (12), does not account satisfactorily for the experimental results. Recall that discrepancies between the theoretical and experimental results were noticed also in the fluorescence spectra from the neon positive column without laser excitation. The numerical analysis of the neon-level populations was based on parameters taken from several sources, and it may be assumed that some parameters must be modified for the condition of our experiment. For instance, the collisional-mixing coefficients $K_{ij}^{(s)}$ and $K_{ij}^{(p)}$ are taken without modifications from Refs. 20 and 24, respectively. If the collisional mixing coefficients are appropriately modified, the discrepancies in the fluorescence spectra may be removed. However, our data base is not large enough to determine accurately all those collisional coefficients.

CONCLUSIONS

We have presented a simultaneous investigation of the OG effect and laser-induced spectra of the $1s_i$–$2p_j$ transitions in a neon positive column. An OG model, an extension of the Doughty and Lawler OG model, has been introduced to analyze the experimental results. Our model is based on a set of steady-state rate equations describing the populations of the four $1s_i$ levels, the ten $2p_j$ levels, and the electron density. Comparison between the theoretical and experimental OG signal was good for various laser-excited neon transitions.

LIF measurements confirmed the key role played by metastable neon atoms in the sustainment of the discharge. Nevertheless, by using electron-impact and collisional-mixing coefficients reported in the literature, our model has not been able to interpret completely the laser-induced spectra.

At first it may appear surprising that the OG spectrum presents a better theory-to-experiment agreement than the fluorescence spectra. This result, however, shows that only the populations of the metastable and radiative $1s_i$ levels determine the OG signal, and the OG signal is relatively independent of the detail of the $2p_j$ population distribution. This behavior may be different for the OG spectrum at large discharge current, where $2p_j$ electron ionization contributes significantly to the discharge current. In those conditions accurate values of the metastable electron-impact excitation and $1s_i/2p$ collisional-mixing coefficients may be required to analyze both OG and fluorescence spectra.

ACKNOWLEDGMENTS

We wish to thank Pina Di Vito for preliminary results on the OG spectra and J. J. Leventhal for a careful reading of the manuscript. This research was supported by the Gruppo Nazionale Struttura della Materia, Italy.

REFERENCES

1. J. E. Lawler, A. I. Ferguson, J. E. M. Goldsmith, D. J. Jackson, and A. L. Schawlow, Phys. Rev. Lett. **42**, 1046 (1979).
2. For a review see the papers published in J. Phys. C **7**(44) (1983).
3. E. Arimondo, G. Di Vito, K. Ernst, and M. Inguscio, Opt. Lett. **9**, 530 (1984).
4. K. C. Smyth and P. K. Schenck, Chem. Phys. Lett. **55**, 466 (1978).
5. E. F. Zalenski, R. A. Keller, and R. Engleman, J. Chem. Phys. **70**, 1015 (1979).
6. J. E. Lawler, Phys. Rev. A **22**, 1025 (1980).
7. C. Dreze, Y. Demers, and J. M. Gagné, J. Opt. Soc. Am. **72**, 912 (1982).
8. E. Arimondo, M. G. Di Vito, K. Ernst, and M. Inguscio, J. Phys. C **7**, 267 (1983); K. C. Smyth and P. K. Schenck, Chem. Phys. Lett. **55**, 466 (1978).
9. R. Shuker, A. Ben Amar, and G. Erez, Opt. Commun. **42**, 29 (1982).
10. N. Uchimoti, T. Nakajima, S. Maeda, and C. Hirose, Opt. Commun. **44**, 154 (1983).
11. A. Von Engel, *Ionized Gases* (Clarendon, Oxford, 1965).
12. D. K. Doughty and J. E. Lawler, Phys. Rev. A **28**, 773 (1983).
13. K. C. Smith, R. A. Keller, and F. F. Crim, Chem. Phys. Lett. **55**, 473 (1978).
14. D. M. Kane, J. Appl. Phys. **56**, 1267 (1984).
15. K. Tachibana and A. V. Phelps, Phys. Rev. A **36**, 999 (1987).
16. M. H. Phillips, L. W. Anderson, and Chun C. Lin, Phys. Rev. A **32**, 2117 (1985).
17. R. M. Smits and M. Prins, Physica **96C**, 262 (1979).
18. S. N. Salinger and J. E. Rowe, J. Appl. Phys. **39**, 4299 (1969).
19. A. V. Phelps and J. P. Molnar, Phys. Rev. **89**, 1202 (1953).
20. T. Dote and Y. Ichikawa, J. Phys. Soc. Jpn. Lett. **40**, 1217 (1976).
21. C. Brown, *Basic Data of Plasma Physics* (Wiley, New York, 1959), p. 65.
22. W. L. Wiese and G. A. Martin, in *Wavelengths and Transition Probabilities for Atoms and Atomic Ions*, Nat. Stand. Ref. Data Ser., Nat. Bur. Stand. **68**, 386 (1980).
23. T. Holstein, Phys. Rev. **72**, 1212 (1947); **83**, 1159 (1951).
24. A. V. Phelps, Phys. Rev. **114**, 1011 (1959).
25. A. J. Dixon, M. F. A. Harrison, and A. C. H. Smith, in *Abstract of the Eighth International Conference on the Physics of Electronic and Atomic Collisions*, B. C. Cobic and M. V. Kurepa, eds. (Institute of Physics, Belgrade, 1973), Vol. 1, p. 405.
26. N. Van Schaik, L. W. G. Steenhuijsen, P. J. M. Van Bommel, and F. H. P. Verspaget, J. Phys. C **7**, 97 (1979).
27. L. Tonks and I. Langmuir, Phys. Rev. **34**, 876 (1929).
28. A. Corney, *Atomic and Laser Spectroscopy* (Clarendon, Oxford, 1977).
29. J. Dutton, J. Phys. Chem. Ref. Data **4**, 577 (1975).